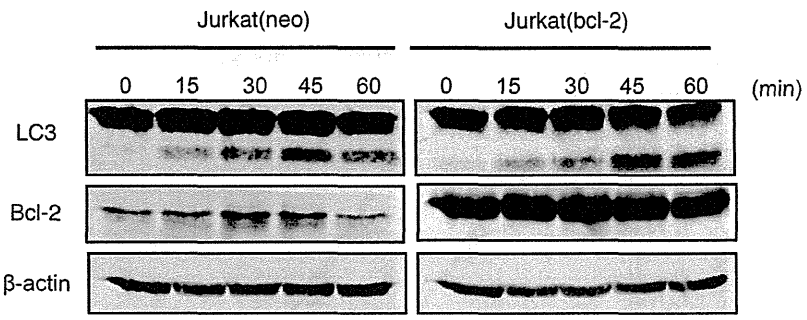

Fig. 4. Overexpression of Bcl-2 did not inhibit RID-B-induced autophagy. Jurkat (neo) and Jurkat (Bcl-2) cells were incubated with 0.4 μM RID-B for the indicated times. The switch of LC3-I to LC3-II was detected by Western blotting. β-Actin was detected as equal protein loading.

crease of LC3-II in a time-dependent manner was observed (Fig. 2B). We also estimated autophagic flux, which is important to distinguish increased autophagosome formation from impaired degradation. Addition of protease inhibitors pepstatin A/E-64-d for blocking lysosome activity further increased RID-B induced LC3-II protein level (Fig. 2C), indicating that autophagy was induced by the RID-B treatment (Fig. 2B).

We also identified another autophagy-related protein. During conventional autophagy, Beclin 1 contributes to progress autolysosome conformation [5]. Here, RID-B treatment did not increase the Beclin 1 level, suggesting that Beclin 1 is not involved in RID-B-induced autophagy (Fig. 2B).

3.3. RID-B-induced autophagy is independent of Bcl-2

In our previous study, we revealed that overexpression of the mitochondria-localized anti-apoptotic protein Bcl-2 in Jurkat cells overcame RID-B-induced apoptosis at 4 μM in a short period of time, 4 h [17]. As shown in Fig. 3A, the overexpression of Bcl-2 clearly inhibited the RID-B-induced decrease in cell viability even after long-term treatment (24 h). At doses of 0.4 μM, the viability of Jurkat cells dropped to 60%, since Bcl-2-overexpressed cells were not damaged at all. Moreover, the overexpression of Bcl-2 blocked the RID-B-induced fragmentation of DNA (Fig. 3B), indicating that Bcl-2 overexpression certainly inhibited RID-B-induced apoptosis.

Bcl-2 binds to Beclin 1 and inhibits conventional autophagy pathway [9,10]. We therefore determined whether Bcl-2 overexpression inhibits RID-B-induced autophagy. As shown in Fig. 4, Bcl-2 overexpression did not alter RID-B-induced LC3-II conversion compared to the control cell line. This result confirms that RID-B-induced autophagy is independent of Beclin 1, and that the RID-B-induced autophagy pathway is different from the conventional autophagy pathway.

4. Discussion

In this study, we treated ER-negative Jurkat cells with the novel tamoxifen derivative RID-B and observed RID-B-induced autophagy at a very low RID-B dose (0.4 μM). During RID-B-induced autophagy, the Beclin 1 level was unchanged. Moreover, overexpression of the mitochondria-localized anti-apoptotic protein Bcl-2 suppressed RID-B-induced cell death, but not autophagy. These results suggested that mitochondria perturbation, which is a main factor in RID-B-induced apoptosis, is not involved in RID-B-induced autophagy, and that RID-B-induced autophagy is different from the conventional autophagy pathway.

In our recent study, we discovered that sub-micromolar doses of RID-B could quickly induce apoptosis despite ER expression. In the present study, low-dose (0.4–0.5 μM) RID-B was administered to ER-negative cells (Jurkat) and ER-positive cells (HepG2), and both cell lines then showed typical LC3 conversion, suggesting that RID-B-induced autophagy is ER-independent, similar to RID-B-induced apoptosis. The original compound tamoxifen also induces autophagy. Schoenlein et al. and others reported that tamoxifen induced autophagy in ER alpha cells [22], but there are no such reports with ER-negative cells, to our knowledge. In the present study, the tamoxifen derivative RID-B induced autophagy despite an ER defect.

Poirot et al. reported that tamoxifen accumulates free sterol and leads to autophagy [23]. In the case of Niemann–Pick disease, cholesterol accumulation resulted in autophagy [24]. Similarly, we found that RID-B accumulated free sterol in HepG2 cells (data not shown). Further studies are needed to determine the involvement of sterol accumulation in RID-B-induced autophagy, and they may clarify the ER independence of the RID-B-induced autophagy pathway.

In our previous study, RID-B-induced apoptosis was mediated by mitochondria perturbation [17]. Bcl-2 overexpression inhibited RID-B-induced apoptosis phenomena including a mitochondria membrane potential decrease, caspase activation and DNA fragmentation. However, Bcl-2 overexpression did not overcome RID-B-induced autophagy. These results suggest that mitochondria perturbation, which is a main factor in RID-B-induced apoptosis, is not involved in RID-B-induced autophagy.

Autophagy signaling machinery is related mainly to the inhibition of the mTOR pathway, which regulates cell growth and cell proliferation [8]. Inhibition of mTOR induced Beclin 1 upregulation, stimulating conventional autophagy process [25]. Moreover, Bcl-2 binds to Beclin 1 and inhibits this conventional autophagy pathway independent of its anti-apoptotic role [9,10]. In the present study, RID-B did not alter the Beclin 1 level at all (Fig. 2). In addition, Bcl-2 overexpression did not inhibit LC3-II conversion. These results suggest that RID-B-induced autophagy is not related to the conventional autophagy pathway, which is independent of Beclin 1.

The so-called noncanonical autophagy pathway forms autophagosomes independent of Beclin 1 and Vps34, involving LC3 [26]. Moreover, the noncanonical autophagy pathway cannot be inhibited by the PI3 K inhibitor 3-methyladenine. We have observed that RID-B-induced LC3 conversion was not inhibited by 3-methyladenine (data not shown). In light of the above findings, the RID-B-induced autophagy pathway seems to be noncanonical, which is independent of Bcl-2 and Beclin 1. Other drugs have induced similar autophagy pathways (Beclin 1-independent) [27,28].

We have observed that RID-B-induced autophagy can occur in various types of cancer cells, without dependency on ER and Bcl-2 levels. Further studies should be conducted to determine the mechanisms underlying RID-B-induced autophagy, to clarify

whether RID-B will be a clinically useful, ER-independent chemotherapeutic agent for cancer.

Acknowledgments

This study was supported by a Health and Labour Sciences Research Grants from the Ministry of Health, Labour and Welfare, Japan. We are thankful of Mr. Takashi Takashima and Mr. Atsushi Takano for technical assistance.

References

[1] N. Mizushima, Autophagy: process and function, Genes Dev. 21 (2007) 2861–2873.
[2] T. Shintani, D.J. Klionsky, Autophagy in health and disease: a double-edged sword, Science 306 (2004) 990–995.
[3] A.M. Cuervo, Autophagy: in sickness and in health, Trends Cell Biol. 14 (2004) 70–77.
[4] D. Mijaljica, M. Prescott, D.J. Klionsky, R.J. Devenish, Autophagy and vacuole homeostasis: a case for self-degradation?, Autophagy 3 (2007) 417–421
[5] S.F. Funderburk, Q.J. Wang, Z. Yue, The Beclin 1-VPS34 complex–at the crossroads of autophagy and beyond, Trends Cell Biol. 20 (2010) 355–362.
[6] S. Pankiv, T.H. Clausen, T. Lamark, A. Brech, J.A. Bruun, H. Outzen, A. Overvatn, G. Bjorkoy, T. Johansen, P62/SQSTM1 binds directly to Atg8/LC3 to facilitate degradation of ubiquitinated protein aggregates by autophagy, J. Biol. Chem. 282 (2007) 24131–24145.
[7] S. Pattingre, L. Espert, M. Biard-Piechaczyk, P. Codogno, Regulation of macroautophagy by mTOR and Beclin 1 complexes, Biochimie 90 (2008) 313–323.
[8] T. Yorimitsu, D.J. Klionsky, Eating the endoplasmic reticulum: quality control by autophagy, Trends Cell Biol. 17 (2007) 279–285.
[9] S. Pattingre, A. Tassa, X. Qu, R. Garuti, X.H. Liang, N. Mizushima, M. Packer, M.D. Schneider, B. Levine, Bcl-2 antiapoptotic proteins inhibit Beclin 1-dependent autophagy, Cell 122 (2005) 927–939.
[10] S. Oh, E. Xiaofei, D. Ni, S.D. Pirooz, J.Y. Lee, D. Lee, Z. Zhao, S. Lee, H. Lee, B. Ku, T. Kowalik, S.E. Martin, B.H. Oh, J.U. Jung, C. Liang, Downregulation of autophagy by Bcl-2 promotes MCF7 breast cancer cell growth independent of its inhibition of apoptosis, Cell Death Differ. 18 (2011) 452–464.
[11] A.C. Kimmelman, The dynamic nature of autophagy in cancer, Genes Dev. 25 (2011) 1999–2010.
[12] A. Notte, L. Leclere, C. Michiels, Autophagy as a mediator of chemotherapy-induced cell death in cancer, Biochem. Pharmacol. 82 (2011) 427–434.
[13] G. Xi, X. Hu, B. Wu, H. Jiang, C.Y. Young, Y. Pang, H. Yuan, Autophagy inhibition promotes paclitaxel-induced apoptosis in cancer cells, Cancer Lett. 307 (2011) 141–148.
[14] Y.K. Jo, S.J. Park, J.H. Shin, Y. Kim, J.J. Hwang, D.H. Cho, J.C. Kim, ARP101, a selective MMP-2 inhibitor, induces autophagy-associated cell death in cancer cells, Biochem. Biophys. Res. Commun. 404 (2011) 1039–1043.
[15] P. de Medina, S. Silvente-Poirot, M. Poirot, Tamoxifen and AEBS ligands induced apoptosis and autophagy in breast cancer cells through the stimulation of sterol accumulation, Autophagy 5 (2009) 1066–1067.
[16] K.S. Cho, Y.H. Yoon, J.A. Choi, S.J. Lee, J.Y. Koh, Induction of autophagy and cell death by tamoxifen in cultured retinal pigment epithelial and photoreceptor cells, Invest. Ophthalmol. Vis. Sci. 53 (2012) 5344–5353.
[17] Y. Nagahara, I. Shiina, K. Nakata, A. Sasaki, T. Miyamoto, M. Ikekita, Induction of mitochondria-involved apoptosis in estrogen receptor-negative cells by a novel tamoxifen derivative, ridaifen-B, Cancer Sci. 99 (2008) 608–614.
[18] I. Shiina, Y. Sano, K. Nakata, M. Suzuki, T. Yokoyama, A. Sasaki, T. Orikasa, T. Miyamoto, M. Ikekita, Y. Nagahara, Y. Hasome, An expeditious synthesis of tamoxifen, a representative SERM (selective estrogen receptor modulator), via the three-component coupling reaction among aromatic aldehyde, cinnamyltrimethylsilane, and beta-chlorophenetole, Bioorg. Med. Chem. 15 (2007) 7599–7617.
[19] I. Shiina, Y. Sano, K. Nakata, T. Kikuchi, A. Sasaki, M. Ikekita, Y. Nagahara, Y. Hasome, T. Yamori, K. Yamazaki, Synthesis and pharmacological evaluation of the novel pseudo-symmetrical tamoxifen derivatives as anti-tumor agents, Biochem. Pharmacol. 75 (2008) 1014–1026.
[20] H.E. Polson, J. de Lartigue, D.J. Rigden, M. Reedijk, S. Urbe, M.J. Clague, S.A. Tooze, Mammalian Atg18 (WIPI2) localizes to omegasome-anchored phagophores and positively regulates LC3 lipidation, Autophagy (6) (2010).
[21] Y. Kabeya, N. Mizushima, T. Ueno, A. Yamamoto, T. Kirisako, T. Noda, E. Kominami, Y. Ohsumi, T. Yoshimori, LC3, a mammalian homologue of yeast Apg8p, is localized in autophagosome membranes after processing, EMBO J. 19 (2000) 5720–5728.
[22] P.V. Schoenlein, S. Periyasamy-Thandavan, J.S. Samaddar, W.H. Jackson, J.T. Barrett, Autophagy facilitates the progression of ERalpha-positive breast cancer cells to antiestrogen resistance, Autophagy 5 (2009) 400–403.
[23] M. Poirot, S. Silvente-Poirot, R.R. Weichselbaum, Cholesterol metabolism and resistance to tamoxifen, Curr. Opin. Pharmacol. 12 (2012) 683–689.
[24] S. Ishibashi, T. Yamazaki, K. Okamoto, Association of autophagy with cholesterol-accumulated compartments in Niemann–Pick disease type C cells, J. Clin. Neurosci. 16 (2009) 954–959.
[25] S. Carloni, S. Girelli, C. Scopa, G. Buonocore, M. Longini, W. Balduini, Activation of autophagy and Akt/CREB signaling play an equivalent role in the neuroprotective effect of rapamycin in neonatal hypoxia-ischemia, Autophagy 6 (2010) 366–377.
[26] K. Juenemann, E.A. Reits, Alternative macroautophagic pathways, Int. J. Cell. Biol. 2012 (2012) 189794.
[27] F. Scarlatti, R. Maffei, I. Beau, P. Codogno, R. Ghidoni, Role of non-canonical Beclin 1-independent autophagy in cell death induced by resveratrol in human breast cancer cells, Cell Death Differ. 15 (2008) 1318–1329.
[28] D.M. Smith, S. Patel, F. Raffoul, E. Haller, G.B. Mills, M. Nanjundan, Arsenic trioxide induces a beclin-1-independent autophagic pathway via modulation of SnoN/SkiL expression in ovarian carcinoma cells, Cell Death Differ. 17 (2010) 1867–1881.

Highlighted Paper selected by Editor-in-Chief

Search for Novel Anti-tumor Agents from Ridaifens Using JFCR39, a Panel of Human Cancer Cell Lines

Wen-zhi Guo,[a] Yanwen Wang,[b] Eri Umeda,[b] Isamu Shiina,[b] Shingo Dan,[a] and Takao Yamori*[,a,c]

[a] *Division of Molecular Pharmacology, Cancer Chemotherapy Center, Japanese Foundation for Cancer Research; 3–8–31 Ariake, Koto-ku, Tokyo 135–8550, Japan:* [b] *Department of Applied Chemistry, Faculty of Science, Tokyo University of Science; 1–3 Kagurazaka, Shinjuku-ku, Tokyo 162–0860, Japan: and* [c] *Center for Product Evaluation, Pharmaceuticals and Medical Devices Agency; 3–3–2 Kasumigaseki, Chiyoda-ku, Tokyo 100–0013, Japan.*

Received February 11, 2013; accepted April 2, 2013; advance publication released online April 9, 2013

To overcome the heterogeneous nature of cancer, the search for potent anti-cancer drug candidates with new modes of action is essential. For that purpose, we prepared forty-eight Ridaifens (RIDs), a novel series of tamoxifen-derivatives. Then, we screened them, searching for novel candidates for a new class of anti-cancer drug using a panel of human cancer cell lines (JFCR39) and by a binding assay to estrogen receptor α (ERα). First, the growth inhibition of the forty-eight RIDs against JFCR39 was evaluated. Forty RIDs showed higher growth-inhibitory activity than that of tamoxifen. The structure–activity relationship (SAR) study revealed that the aminoalkoxyphenyl groups at the C-1 position and the common central ethylenic bond were important in retaining a high level of growth-inhibitory activity. Subsequently, the ERα binding activity of all the RIDs was measured by a competitive binding assay. The SAR study for ERα binding activity indicated that both the phenyl group and the ethyl group at the C-2 position in the ethylenic bond were essential. Based on the screenings, we identified RID-SB1 and RID-SB8, which demonstrated potent tumor growth inhibition but had completely lost ERα binding activity. Furthermore, the COMPARE analysis using JFCR39 suggested that RID-SB1 and RID-SB8 had different molecular modes of action compared to those of the current anti-cancer drugs including tamoxifen. These results indicate that RID-SB1 and RID-SB8 are interesting candidates for novel anti-cancer agents with unique modes of action.

Key words tamoxifen-derivative; anti-cancer; JFCR39 panel; Ridaifen; novel mechanism; drug discovery

Tamoxifen is an antagonist of the estrogen receptor (ER). It has been used as the first-line agent for breast cancer for more than 30 years although competitive estrogen inhibitors have been developed to treat hormonally responsive breast cancer.[1–3] The accumulative risk-benefit assessment of tamoxifen therapy has established its efficacy and safety.[4–6] Many studies of the action mode of tamoxifen have been done, which have revealed that tamoxifen is not only an estrogen blocker but also a modulator of various signaling proteins located in ER-independent biological pathways; for example protein kinase C (PKC), calmodulin, transforming growth factor β and protooncogene c-myc. Interestingly, it has been suggested that other molecules, such as caspases, mitogen-activated protein kinases (MAPK), c-Jun N-terminal kinase (JNK) and p38, are involved in tamoxifen-induced apoptotic signaling.[7,8] These reports indicate that tamoxifen potentially acts on multiple targets. Therefore, tamoxifen can be used as a lead compound to produce a new generation of anti-cancer drug with a unique mode of action, which will be used for other cancers in addition to breast cancer.

We developed a new efficient synthetic method for tamoxifen *via* a three-component coupling reaction.[9] Then we synthesized a series of tamoxifen derivatives, designated as Ridaifens (RIDs), expecting that they would display a variety of biological activities. As expected, we demonstrated the anti-tumor activity of three RIDs, RID-B, C, and D.[10] In this study, we further modified the structure of tamoxifen, and obtained a new series of RIDs consisting of forty-eight RIDs over three generations of modifications.

To identify anti-cancer drug candidates that have potentially unique modes of action, we had previously established a panel of 39 human cancer cell lines, designated as JFCR39, which was coupled to an anti-cancer drug activity database and a computer algorithm COMPARE.[11–13] This system provides rich and fundamental information on the pharmacological action modes of chemicals on cancer cells. The COMPARE algorithm enabled us to identify novel drug candidates with potentially unique modes of action compared to current anti-cancer drugs. Moreover, it sometimes predicted the molecular targets or the modes of action of novel compounds. Indeed, by running the JFCR39 system and COMPARE, we successfully identified novel anti-cancer agents, such as a telomerase inhibitor (FJ-5002),[14] a topoisomerase I/II inhibitor (MS247),[15] a phosphatidylinositol 3-kinase inhibitor (ZSTK474),[16–18] a Golgi inhibitor (AMF-26)[19] and so on.

In the present study, we screened the forty-eight RIDs with the JFCR39 panel to identify compound that have potent growth-inhibitory activity and unique modes of action. We also evaluated the RIDs for their estrogen receptor (ER) binding activity to identify compounds which have lost ER binding activity. As a result, we found two RIDs, RID-SB1 and RID-SB8, that had potent growth-inhibitory activity against JFCR39 and had lost ERα binding activity.

MATERIALS AND METHODS

Chemicals Forty-eight RIDs were synthesized over three generations of modifications. The 1st-generation of RIDs is shown in Fig. 1A. When aminoalkyl group R of the RID was R^A, R^B, R^C, R^D, R^E, R^F, R^G or R^H, each derivative was named as RID-A, RID-B, RID-C, RID-D, RID-E, RID-F, RID-G or RID-H, respectively. The 2nd-generation RIDs are based

The authors declare no conflict of interest.

* To whom correspondence should be addressed. e-mail: yamori@jfcr.or.jp

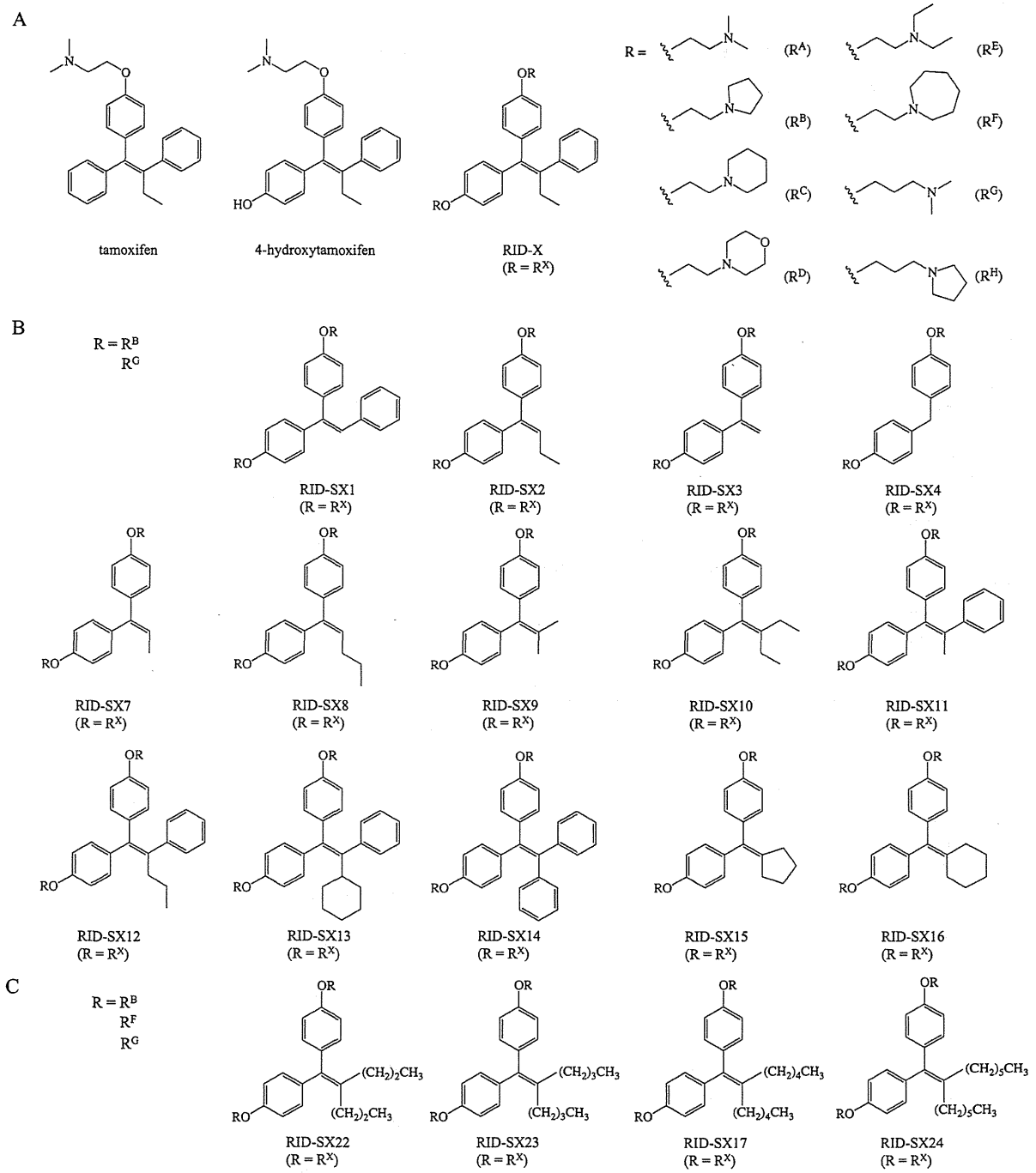

Fig. 1. Chemical Structures of Tamoxifen, 4-Hydroxytamoxifen and RIDs

(A) Tamoxifen, 4-hydroxytamoxifen and first-generation RIDs. (B) Second-generation RIDs. (C) Third-generation RIDs.

on modifications of the ethylene moiety in the 1st-generation RIDs (Fig. 1B). There are two types of the 2nd-generation RIDs, which include R^B or R^G for the aminoalkyl group R. For example, RID-SB1 has aminoalkyl group R^B as a side-chain and RID-SG1 has aminoalkyl group R^G as a side-chain. The 3rd-generation RIDs possess two identical alkyl chains ($\geq C_3$ (propyl) group) at the C-2 position, giving rise to symmetrical structures. There are three types of the 3rd-generation RIDs, bearing R^B, R^F or R^G for the aminoalkyl group R (Fig. 1C). 4-Hydroxytamoxifen and tamoxifen were purchased from Sigma (St. Louis, U.S.A.). The physical properties of RID-SB1 and RID-SB8 and their ^{1}H- and ^{13}C-NMR charts were indicated in Supplemental information 1.

Cell Lines A panel of 39 human cancer cell lines, known as JFCR39, containing the following cell lines: lung cancer, NCI-H23, NCI-H226, NCI-H522, NCI-H460, A549, DMS273 and DMS114; colorectal cancer, HCC-2998, KM-12, HT-29, HCT-15 and HCT-116, gastric cancer, MKN-1, MKN-7, MKN-28, MKN-45, MKN-74, St-4; ovarian cancer, OVCAR-3, OVCAR-4, OVCAR-5, OVCAR-8 and SK-OV-3; breast cancer, BSY-1, HBC-4, HBC-5, MDA-MB-231 and MCF-7; renal cancer, RXF-631L and ACHN; melanoma, LOX-IMVI; glioma,

U251, SF-295, SF539, SF268, SNB75 and SNB78; prostate cancer, DU-145 and PC-3, was used as described previously (1–3). All the cell lines were cultured in RPMI 1640 medium supplemented with 5% (v/v) fetal bovine serum, penicillin (100 U/mL) and streptomycin (100 mg/mL) at 37°C in a humidified atmosphere containing 5% (v/v) CO_2.

Determination of Cell Growth Inhibition Profiles (Fingerprint) Inhibition of cell growth was assessed by the change in total cellular protein following 48 h of treatment with a given test compound, and was measured using the sulforhodamine B (SRB) assay as described previously.[20] The 50% growth inhibition (GI_{50}) value of the drug was calculated as described previously.[21] A graphic representation (termed fingerprint) of the differential growth inhibition of each compound for the cells in the JFCR39 panel was plotted based on a calculation employing a set of GI_{50} values.[22]

COMPARE Analysis We used COMPARE analysis to assess two compounds for the similarity of their mode of action based on their fingerprints. COMPARE analysis was performed by calculating the Pearson correlation coefficient (r) between the GI_{50} mean graphs of the compounds X and Y using the following formula: $r=(\sum(x_i-x_m)(y_i-y_m))/(\sum(x_i-x_m)^2\sum(y_i-y_m)^2)^{1/2}$, where x_i and y_i are Log GI_{50} of the two compounds, respectively, for each cell line, and x_m and y_m are the mean values of x_i and y_i, respectively (n=39).[22] The Pearson correlation coefficients were used to determine the degree of similarity. The greater the coefficient is, the higher the similarity between X and Y.

Estrogen Receptor Binding Affinity Assay The ERα binding affinity assay was performed using recombinant ERα (Thermo, Massachusetts, U.S.A.) and the HitHunter Enzyme Fragment Complementary (EFC) Estrogen Receptor Assay kit (Discoverx Corporation, Fremont, CA, U.S.A.) according to the manufacturer's protocol.[23] HitHunter EFC technology is based on a genetically engineered β-galactosidase enzyme that consists of two fragments termed enzyme acceptor (EA) and enzyme donor conjugated with estradiol (ED-estradiol). Briefly, different concentrations of RIDs were added to wells containing recombinant ERα and ED-estradiol in a 384-well white plate and incubated for 1.5 h. ED-estradiol competes with RIDs in binding to ER. Any unbound ED-estradiol conjugates with EA to form an active β-galactosidase enzyme, which subsequently hydrolyzes the fluorescent substrate for luminescent detection by a microplate reader (Bio-Rad, California, U.S.A.). The excitation wavelength is 530 nm and luminosity is detected at 620 nm. The competition activity was calculated using the following formula: percent competition=(X-positive ER control)/(negative ER control-positive ER control)×100%, where X is the value of luminescent detection of RIDs. A standard curve of estradiol was run in parallel. All assays were performed in triplicates.

RESULTS

Growth-Inhibitory Activities of RIDs against JFCR39 The growth-inhibitory activities of forty-eight RIDs against JFCR39 were determined by SRB assay as described in Materials and Methods. Figure 2 shows the dose response curves of the cells in the JFCR39 panel against tamoxifen and RID-SB1 as examples. The concentration at which the cell growth is inhibited by 50% represents GI_{50}. Supplemental information 2 summarizes the GI_{50} values of the forty-eight RIDs against each cancer cell line in JFCR39. The mean value of GI_{50} over all 39 cell lines (designated as MG-MID) is summarized in Table 1. The MG-MID of the RIDs ranged from 0.85 μM (RID-G) to 43.7 μM (RID-SB4). Based on the MG-MID, we found that forty of the forty-eight RIDs showed higher proliferation inhibition than tamoxifen (MG-MID=7.41 μM).

The 1st-generation RIDs each have a pair of identical substituents (-OR) on the phenyl groups bound to the central ethylene moiety at the C-1 position (Fig. 1A). Here, the aminoalkoxy substituents were modified without changing the structures of the third phenyl group and the ethyl group at the C-2 position. The 1st-generation RIDs all showed higher antitumor activity than tamoxifen, except RID-D (MG-MID= 14.8 μM). These results indicate that the modifications of aminoalkyl group R with R^A–R^H except R^D enhanced the growth-inhibitory activity.

All the 2nd- and 3rd-generation RIDs have two identical aminoalkoxy substituents on both phenyl groups at the C-1 position (Figs. 1B, C). We selected a number of representative aminoalkyl groups for the generation of further variations of RIDs (R=R^B or R^G in the 2nd-generation; R=R^B, R^F or R^G in the 3rd-generation). The central ethylenic bond was then either removed (S4 type in Fig. 1B), or modified with two substituents at the C-2 position. The S4 type RIDs showed remarkably reduced activities compared to tamoxifen (MG-MID=7.41 μM) and all other RIDs. The MG-MIDs of RID-SB4 and RID-SG4 were 43.7 μM and 26.3 μM, respectively (Table 1). These results indicate that the central ethylenic bond is important for enhancing growth-inhibitory activity. On the other hand, most of the RIDs with modifications to the two C-2 substituents on the central ethylene bond did not exhibit a significant change in their growth-inhibitory activity compared to 1st-generation RIDs. The 3rd-generation RIDs have completely symmetrical structures, in which two identical alkyl chains of various lengths (C3–C6) are bound to the central ethylenic moiety. Most of them retain high levels of growth-inhibitory activity.

Each test compound was further characterized by its GI_{50} profile across JFCR39, which was designated as "fingerprint." For example, the fingerprints of tamoxifen and RID-SB1 and RID-SB8 (Supplemental information 1) were shown in Fig. 3. According to the analysis by COMPARE, the correlation coefficients between the fingerprints of tamoxifen and RID-SB1, and between tamoxifen and RID-SB8 were 0.199 and 0.318, respectively. These results suggest that RID-SB1 and RID-SB8 are different from tamoxifen with respect to their mode of action. Indeed, these two RIDs exhibited no ERα binding activity (see below).

ERα Binding Activities of RIDs The ERα binding activity of the forty-eight RIDs was determined by the competitive binding of ED-Estradiol to ERα. The competitive binding curves of estradiol (positive control), tamoxifen and 4-hydroxytamoxifen are shown in Fig. 4. The y-axis indicates the percent inhibition of ED-Estradiol binding to ERα. Among the RIDs, RID-G and RID-SB1 indicated the strongest and the lowest ERα binding activity, respectively (Fig. 4).

The IC_{50} values of all of the RIDs are shown in Table 1. The relationship between chemical structure and ERα binding activity was studied here. The 1st-generation RIDs (RID-A–H) with the various substituents on the phenyl rings at the C-1 position yielded IC_{50} values ranging from 26.6 (RID-G)

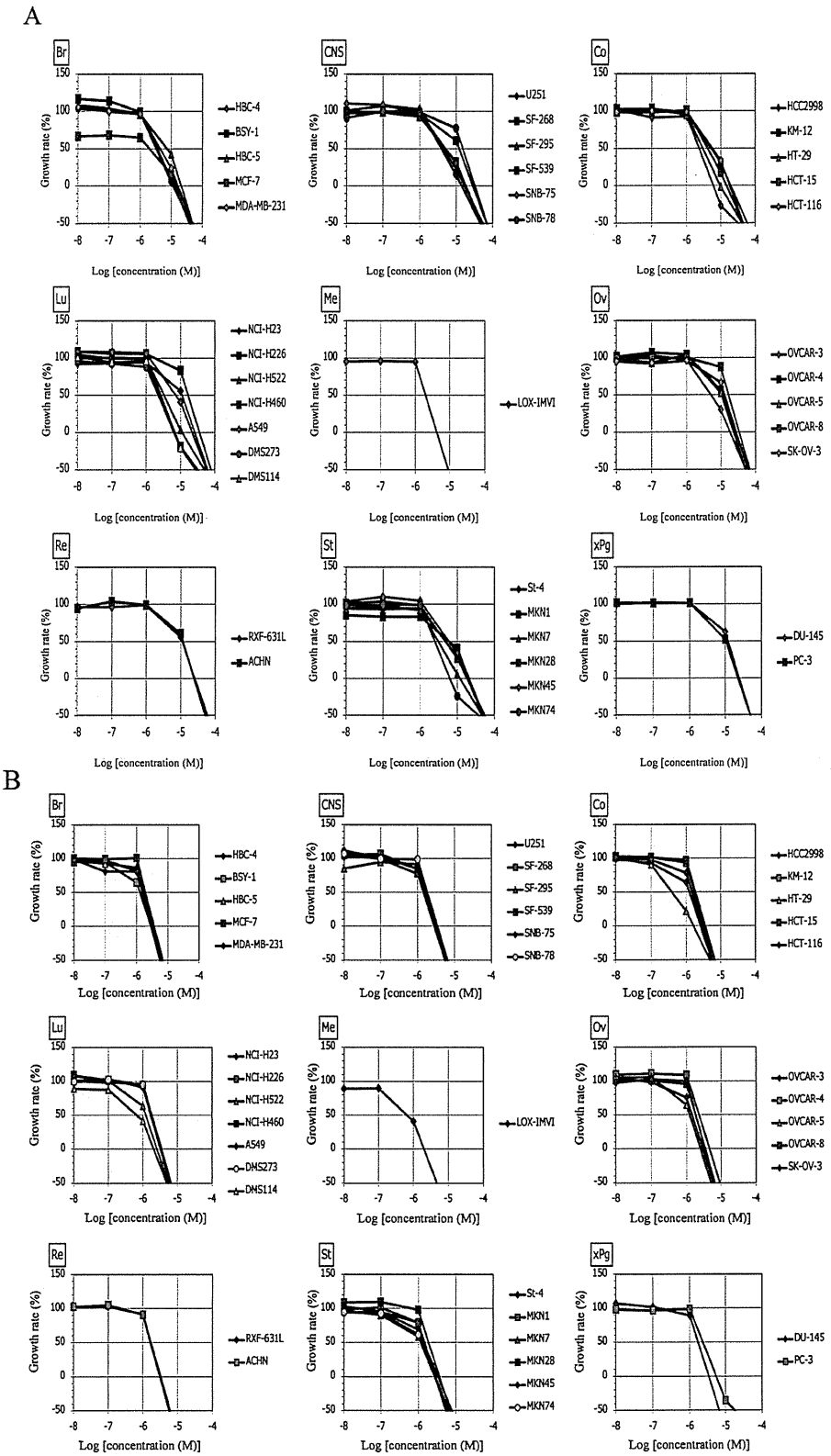

Fig. 2. Dose Response Curves of (A) Tamoxifen and (B) RID-SB1 against Growth of JFCR39 Cancer Cell Lines

The growth inhibition of tamoxifen and RID-SB1 on 39 cell lines (Br, breast; CNS, central nervous system; Co, colorectal; Lu, lung; Me, melanoma; Ov, ovarian; Re, renal; St, stomach; xPg, prostate) were measured as described in Materials and Methods.

Table 1. Anti-tumor Activity and ERα Binding Capacity of RIDs

Chemical	MG-MID (μM)	ERα binding activity IC_{50} (nM)	Generation	Chemical	MG-MID (μM)	ERα binding activity IC_{50} (nM)	Generation
17β-Estradiol	—	1.89		RID-SG2	15.50	>10000	2nd
4-Hydroxy-tamoxifen	5.50	2.72		RID-SG3	6.46	>10000	2nd
Tamoxifen	7.41	21.1		RID-SG4	26.3	>10000	2nd
RID-A	1.48	171	1st	RID-SG7	17.4	>10000	2nd
RID-B	1.17	52.4	1st	RID-SG8	1.55	2910	2nd
RID-C	3.47	295	1st	RID-SG9	1.82	8570	2nd
RID-D	14.8	47.7	1st	RID-SG10	1.45	372	2nd
RID-E	1.20	320	1st	RID-SG11	1.55	127	2nd
RID-F	2.45	154	1st	RID-SG12	1.38	23.9	2nd
RID-G	0.85	26.7	1st	RID-SG13	1.32	234	2nd
RID-H	1.05	44.1	1st	RID-SG14	1.51	109	2nd
RID-SB1	1.38	>10000	2nd	RID-SG15	1.51	835	2nd
RID-SB2	5.40	>10000	2nd	RID-SG16	1.10	1230	2nd
RID-SB3	10.5	>10000	2nd	RID-SB22	1.51	383	3rd
RID-SB4	43.7	>10000	2nd	RID-SB23	1.70	253	3rd
RID-SB7	5.77	>10000	2nd	RID-SB17	2.00	380	3rd
RID-SB8	1.82	>10000	2nd	RID-SB24	2.63	568	3rd
RID-SB9	2.69	4640	2nd	RID-SF22	1.79	421	3rd
RID-SB10	1.51	2370	2nd	RID-SF23	6.03	656	3rd
RID-SB11	1.44	582	2nd	RID-SF17	12.0	428	3rd
RID-SB12	1.34	145	2nd	RID-SF24	17.0	1840	3rd
RID-SB13	1.31	218	2nd	RID-SG22	1.05	253	3rd
RID-SB14	1.44	280	2nd	RID-SG23	1.70	387	3rd
RID-SB15	1.62	4880	2nd	RID-SG17	1.78	515	3rd
RID-SB16	1.46	702	2nd	RID-SG24	2.04	1560	3rd
RID-SG1	2.29	>10000	2nd				

to 320 nM (RID-E) (Table 1). These results indicated that the structures of substituents on the phenyl rings at the C-1 position in RIDs considerably affected the binding activity to ERα. RID-G showed ERα binding activity almost equal to tamoxifen. However, no RID compound surpassed 4-hydroxytamoxifen, an active form of tamoxifen, in ERα binding activity.

An interesting finding was observed in the ERα binding activities of the 2nd-generation RIDs. These RIDs were used to study the importance of the substituents around the C-2 position of the central ethylenic bond while retaining the two aromatic rings with identical aminoalkoxy groups at C-1. It was observed that the eight RIDs, RID-SB1, SB2, SB3 SB4, SG1, SG2, SG3 and SG4, had completely lost ERα binding activity. Structurally, these RIDs had lost either one or both of the phenyl group or the ethyl group at the C-2 position. These results clearly indicate that the phenyl and ethyl group at the C-2 position in the ethylenic bond are essential. The impact of modifications of the substituents around the ethylenic bond (RID-SB7 to SB16 and RID-SG7 to SG16) was also examined. The ERα binding activity varied significantly (23.89–>10000 nM) depending on the modification. A trend was observed whereby the RIDs having more bulky structures around the double bond (RID-SB7 to SB12 and SG7 to SG12) displayed higher ERα binding activities (Table 1).

The 3rd-generation RIDs (RID-SG22, SG23, SG17, SG24, SB22, SB23, SB17, SB24, SF22, SF23, SF17 and SF24) (Fig. 1C) and some of the 2nd-generation RIDs (RID-SG9, SG10, SB9, SB10, SF9 and SF10) (Fig. 1B) have symmetrical structures. These RIDs showed lower ER binding activity in comparison to the 1st-generation RIDs (Table 1). RID-SG22, SG23, SG17, SG24, SB22, SB23, SB17, SB24, SF22, SF23, SF17 and SF24 (3rd-generation RIDs, Fig. 1C) have longer alkyl chains ($\geq C_3$ (propyl) group) than RID-SG9, SG10, SB9, SB10, SF9 and SF10 (2nd-generation, Fig. 1B), and exhibited greater activities than RID-SG9, SG10, SB9, SB10, SF9 and SF10.

Two RIDs with Notably High ER-Independent Antitumor Activities To evaluate the RIDs in terms of growth-inhibitory activity and ERα binding activity, a scattergram of growth inhibition (x-axis) and ERα binding activity (y-axis) for the RIDs was drawn (Fig. 5). Each spot represents one RID compound and both activities varied over a wide range. Here, we focused on two RIDs, RID-SB1 and RID-SB8 (Supporting Information 1), that had both completely lost ERα binding activity, while exhibiting the high levels of growth-inhibitory activity, suggestive that they inhibited the cell growth *via* an ER-independent mechanism. To confirm this point, we examined the fingerprints of the two RIDs (Fig. 3). The COMPARE analysis of RID-SB1 and RID-SB8 revealed that both of them showed a very weak correlation coefficient ($r < 0.4$) with tamoxifen (Table 2). These results suggest that both RID-SB1 and RID-SB8 have a different pharmacological mode of action to that of tamoxifen.

COMPARE Analysis of RID-SB1 and RID-SB8 We previously established the JFCR39 drug database and COMPARE analysis and demonstrated that this system is a powerful tool for use in identifying the molecular targets or pharmacological modes of action of novel compounds.[11–13] The JFCR39 drug database integrates the fingerprints of reference compounds including 87 standard drugs currently used in clinic and more than 1100 inhibitors of various en-

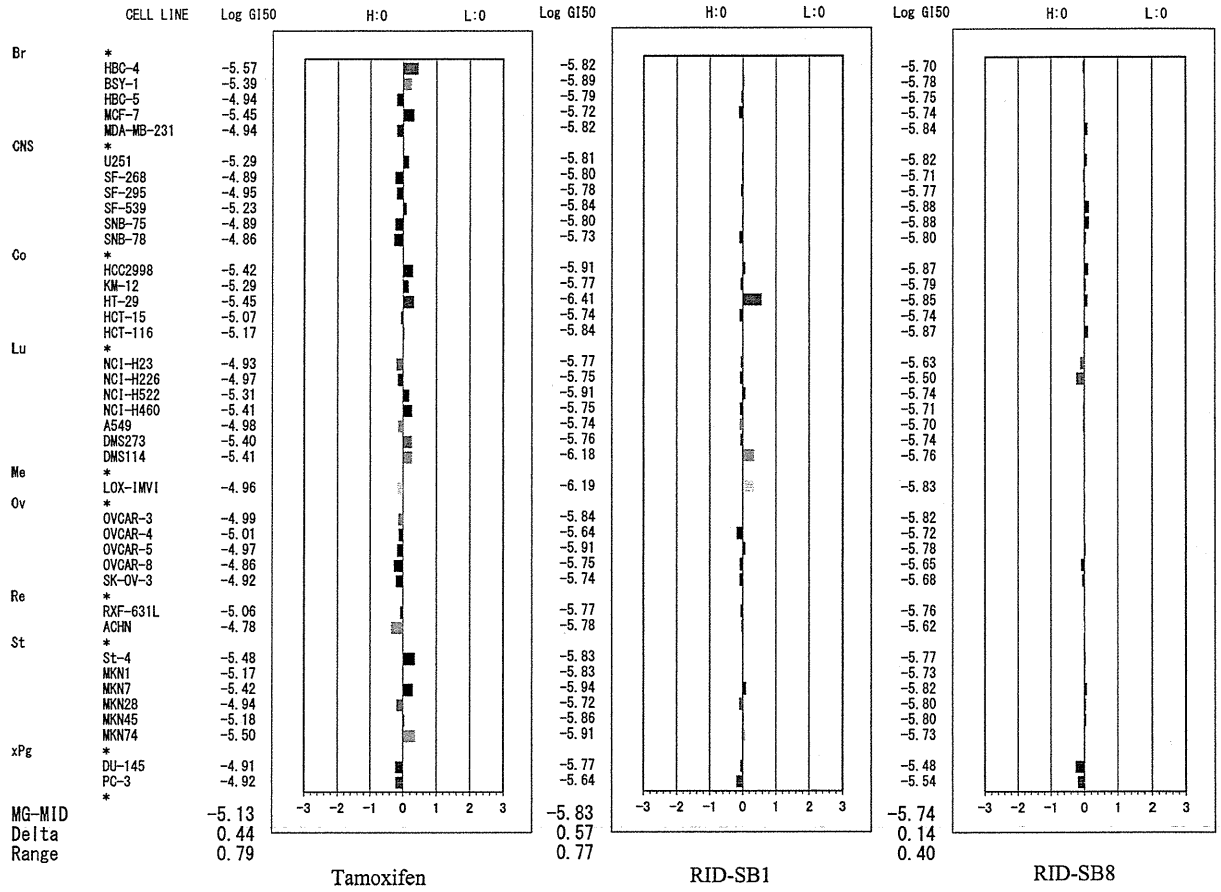

Fig. 3. Fingerprints of Tamoxifen, RID-SB1 and RID-SB8

Fingerprint shows the differential growth inhibition pattern of chemicals against JFCR39 cancer cell lines. The *X*-axis represents difference in logarithmic scale between mean of Log GI_{50} values for 39 cell lines and the Log GI_{50} for each cell line. Bars to the right of 0 indicates cell lines that are sensitive to the compound, in contrast, bars on the left of 0 means the resistance. MG-MID, mean of Log GI_{50} values for 39 cell lines; Delta, difference between the MG-MID and the Log GI_{50} value for the most sensitive cell line; Range, difference between the Log GI_{50} values for the most resistant cell and the most sensitive cell line.

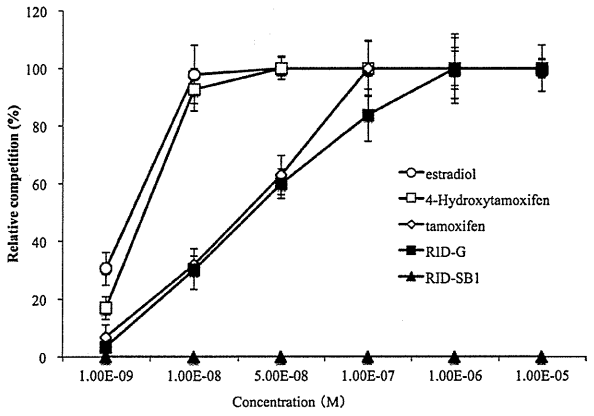

Fig. 4. Competitive Binding Curves of Estradiol, Tamoxifen, 4-Hydroxytamoxifen, RID-SB1 and RID-G

ERα competitive binding activity was measured as described in Materials and Methods. Estradiol, tamoxifen, 4-hydroxytamoxifen, RID-G and RID-SB1 are represented as ○, ◇, □, ■, ▲, respectively.

zymes and biological pathway. To investigate the possible modes of action of RID-SB1 and RID-SB8, we carried out the COMPARE analysis. The two RIDs did not correlate with any currently used anti-cancer drugs (r<0.4). Table 2 summarized the top three reference compounds, which were extracted from the database due to the similarity of their fingerprint profiles to RID-SB1 or RID-SB8. It was indicated that RID-SB1 was most similar to NVP-AEW541 (IGF-1R inhibitor), Bortezomib (proteasome inhibitor) and RDEA119 (MEK inhibitor). RID-SB8 was most similar to PB28 dihydrochloride (sigma-2 receptor agonist), MEK inhibitor I (MEK inhibitor) and Raf 1 Kinase Inhibitor I (Raf 1 kinase inhibitor). Although the correlation coefficients were not high enough, the targets of these reference compounds could be the targets of RID-SB1 or RID-SB8.

DISCUSSION

Tamoxifen performs its anti-tumor activity *via* many pathways, both ER-dependent and ER-independent. In the present study, we attempted to identify novel anti-tumor compounds among RIDs that were designed from a lead compound, tamoxifen. We synthesized forty-eight RIDs by efficient methods including the three-component coupling reaction.[9] To screen them for promising anti-tumor compounds, we used the JFCR39 panel and an ER binding assay. By this means, we found two RIDs, RID-SB1 and RID-SB8, that showed stronger growth-inhibitory activity than tamoxifen and are expected to have unique modes of action.

The forty-eight RIDs showed growth-inhibitory activi-

ties against JFCR39 over a wide range of MG-MIDs from 0.85 to 43.7 μM. Forty out of forty-eight RIDs (83%) showed higher growth-inhibitory activity than tamoxifen (MG-MID= 7.41 μM). The SAR study indicated that the structures of aminoalkoxyphenyl groups at the C-1 position and the common central ethylenic double bond were important in retaining a high level of growth-inhibitory activity.

The ERα binding activity of the RIDs was spread across a huge range of IC_{50} values from 26.7 to >10000 nM. In general, the 1st-generation RIDs exhibited ERα binding activities. Among them RID-G showed the most potent activity (IC_{50}=26.6 nM), which is close to the activity of tamoxifen (IC_{50}=21.1 nM). In contrast, a number of RIDs in the 2nd-generation were inactive with respect to ERα binding. The SAR study clearly indicated that both the phenyl and ethyl groups at the C-2 position of the central ethylenic bond were essential for ERα binding activity. In addition, there was a tendency for RIDs bearing more bulky structures around the double bond (RID-SB7 to SB12 and SG7 to SG12) to display higher ERα binding activity.

According to the above observations, the forty-eight RID compounds were profiled by growth-inhibitory activity and ERα binding activity (Fig. 5). Interestingly, these two activities didn't correlate in the forty-eight RIDs. Some of them, such as RID-G, showed high levels in both activities, while

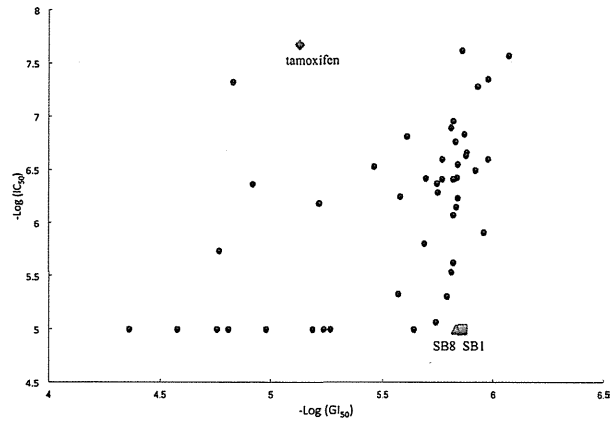

Fig. 5. The Scattergram of RIDs for the Proliferation Inhibition Activity and ERα Binding Activity

The *X*-axis (-MG-MID) represents the proliferation inhibition of forty-eight RIDs in 39 cell lines. The *Y*-axis ($-\mathrm{Log}(IC_{50})$) represents the competitive ERα binding activity. Tamoxifen, RID-SB1 and SB8 are represented as ◇, □, △, respectively.

others were active in only one. In the latter group, we focused on RID-SB1 and RID-SB8 because they were highly active in growth-inhibition but were inactive in regard to ERα binding. It was suggested that they inhibited the cell growth *via* an ER-independent mechanism and thus may inhibit the growth of cancer cells by a different mode of action than tamoxifen. The COMPARE analysis was therefore performed on this study, and it revealed that both RID-SB1 and RID-SB8 showed very weak correlation coefficients ($r < 0.4$) with tamoxifen. These results support the hypothesis above.

So far, a number of tamoxifen derivatives have been designed and synthesized with the aim of enhancing ER binding activity and reducing side-effects. However, this has not been entirely successful. For example, clomifene,[24] ospemifene,[25,26] iodoxifene,[27] raloxifene,[27] arzoxifene,[28] lasofoxifene[29] and levormeloxifene,[30,31] possess high ER binding activity, while still having such disadvantages as biotransformation effect, biological isomerization, thromboembolic effect and agonist action in uterus.[32] Most of these tamoxifen derivatives show very similar effects as tamoxifen and have been proposed considering only the effect on ER. In the present study, RID-SB1 and RID-SB8, while having completely lost ER binding activity, display approximately 5-fold higher antitumor activity than tamoxifen, indicating a non-ER target in its anti-tumor process. Such non-ER function might be useful in unveiling new targets to inhibit tumor cell proliferation. Therefore, RID-SB1 and RID-SB8 maybe novel drug candidates for breast cancer but also for other malignancies.

We finally attempted to predict the action modes of RID-SB1 and RID-SB8 by using our JFCR39 drug database and COMPARE analysis. The two RIDs did not correlate with any currently available anti-cancer drug, suggesting that they could be examples of a novel class of anti-cancer drug. The COMPARE analysis suggested some targets shown in Table 2, however, this needs to be verified by biological testing in the future.

In conclusion, we synthesized forty-eight tamoxifen-derivatives, RIDs, and screened them, searching for novel candidates of a new class of anti-cancer drug. We identified RID-SB1 and RID-SB8 as having potent tumor growth-inhibitory activity but having completely lost ERα binding activity. Based on these results and COMPARE analysis, it was suggested that RID-SB1 and RID-SB8 had unique action modes, different from those of current anti-cancer drugs including tamoxifen. RID-SB1 and RID-SB8 merit further investigation.

Table 2. COMPARE Analysis of RID-SB1 and RID-SB8

Chemical	Ranking	Drug or inhibitor	*r*	Function
RID-SB1	1	NVP-AEW541	0.505	IGF-1R inhibitor
	2	Bortezomib	0.481	Proteasome inhibitor
	3	RDEA119	0.474	MEK inhibitor
	:	:	:	:
	>100	Tamoxifen	0.199	ER antagonist
RID-SB8	1	PB28 dihydrochloride	0.563	sigma-2 Receptor agonist
	2	MEK inhibitor I	0.549	MEK inhibitor
	3	Raf1 Kinase Inhibitor I	0.549	Raf1 inhibitor
	:	:	:	:
	>100	Tamoxifen	0.314	ER antagonist

a) The ID for the chemical in JFCR39 database.

Acknowledgment We thank Dr. R. H. Shoemaker and the late Dr. K. D. Paull for the establishment of JFCR39 and COMPARE analysis, and also thank Ms. Y. Nishimura, Ms. Y. Ohashi, Ms. M. Okamura, Ms. M. Seki, Ms. Y. Mukai and Ms. N. Tamaki for technical assistance.

Grant Support This work was supported by Grants-in-Aid for Scientific Research (A) from Japan Society for the Promotion of Science to TY (22240092), Grant-in-Aid for Scientific Research on Priority Areas from the Ministry of Education, Culture, Sports, Science and Technology to TY (11177101), and a Health and Labour Sciences Research Grants from the Ministry of Health, Labour and Welfare to IS (11103425).

REFERENCES

1) Grainger DJ, Metcalfe JC. Tamoxifen: teaching an old drug new tricks? *Nat. Med.*, **2**, 381–385 (1996).
2) Beekman JM, Allan GF, Tsai SY, Tsai MJ, O'Malley BW. Transcriptional activation by the estrogen receptor requires a conformational change in the ligand binding domain. *Mol. Endocrinol.*, **7**, 1266–1274 (1993).
3) Jordan VC. Molecular mechanisms of antiestrogen action in breast cancer. *Breast Cancer Res. Treat.*, **31**, 41–52 (1994).
4) Catherino WH, Jordan VC. A risk-benefit assessment of tamoxifen therapy. *Drug Saf.*, **8**, 381–397 (1993).
5) Fisher B, Costantino JP, Wickerham DL, Cecchini RS, Cronin WM, Robidoux A, Bevers TB, Kavanah MT, Atkins JN, Margolese RG, Runowicz CD, James JM, Ford LG, Wolmark N. Tamoxifen for the prevention of breast cancer: current status of the National Surgical Adjuvant Breast and Bowel Project P-1 study. *J. Natl. Cancer Inst.*, **97**, 1652–1662 (2005).
6) McDonnell DP. The Molecular Pharmacology of SERMs. *Trends Endocrinol. Metab.*, **10**, 301–311 (1999).
7) Mandlekar S, Kong AN. Mechanisms of tamoxifen-induced apoptosis. *Apoptosis*, **6**, 469–477 (2001).
8) Obrero M, Yu DV, Shapiro DJ. Estrogen receptor-dependent and estrogen receptor-independent pathways for tamoxifen and 4-hydroxytamoxifen-induced programmed cell death. *J. Biol. Chem.*, **277**, 45695–45703 (2002).
9) Shiina I, Sano Y, Nakata K, Kikuchi T, Sasaki A, Ikekita M, Hasome Y. Synthesis of the new pseudo-symmetrical tamoxifen derivatives and their anti-tumor activity. *Bioorg. Med. Chem. Lett.*, **17**, 2421–2424 (2007).
10) Shiina I, Sano Y, Nakata K, Kikuchi T, Sasaki A, Ikekita M, Nagahara Y, Hasome Y, Yamori T, Yamazaki K. Synthesis and pharmacological evaluation of the novel pseudo-symmetrical tamoxifen derivatives as anti-tumor agents. *Biochem. Pharmacol.*, **75**, 1014–1026 (2008).
11) Yamori T. Panel of human cancer cell lines provides valuable database for drug discovery and bioinformatics. *Cancer Chemother. Pharmacol.*, **52** (Suppl. 1), S74–S79 (2003).
12) Nakatsu N, Nakamura T, Yamazaki K, Sadahiro S, Makuuchi H, Kanno J, Yamori T. Evaluation of action mechanisms of toxic chemicals using JFCR39, a panel of human cancer cell lines. *Mol. Pharmacol.*, **72**, 1171–1180 (2007).
13) Dan S, Tsunoda T, Kitahara O, Yanagawa R, Zembutsu H, Katagiri T, Yamazaki K, Nakamura Y, Yamori T. An integrated database of chemosensitivity to 55 anticancer drugs and gene expression profiles of 39 human cancer cell lines. *Cancer Res.*, **62**, 1139–1147 (2002).
14) Naasani I, Seimiya H, Yamori T, Tsuruo T. FJ5002: a potent telomerase inhibitor identified by exploiting the disease-oriented screening program with COMPARE analysis. *Cancer Res.*, **59**, 4004–4011 (1999).
15) Yamori T, Matsunaga A, Sato S, Yamazaki K, Komi A, Ishizu K, Mita I, Edatsugi H, Matsuba Y, Takezawa K, Nakanishi O, Kohno H, Nakajima Y, Komatsu H, Andoh T, Tsuruo T. Potent antitumor activity of MS-247, a novel DNA minor groove binder, evaluated by an *in vitro* and *in vivo* human cancer cell line panel. *Cancer Res.*, **59**, 4042–4049 (1999).
16) Dan S, Okamura M, Seki M, Yamazaki K, Sugita H, Okui M, Mukai Y, Nishimura H, Asaka R, Nomura K, Ishikawa Y, Yamori T. Correlating phosphatidylinositol 3-kinase inhibitor efficacy with signaling pathway status: in silico and biological evaluations. *Cancer Res.*, **70**, 4982–4994 (2010).
17) Kong D, Dan S, Yamazaki K, Yamori T. Inhibition profiles of phosphatidylinositol 3-kinase inhibitors against PI3K superfamily and human cancer cell line panel JFCR39. *Eur. J. Cancer*, **46**, 1111–1121 (2010).
18) Yaguchi S, Fukui Y, Koshimizu I, Yoshimi H, Matsuno T, Gouda H, Hirono S, Yamazaki K, Yamori T. Antitumor activity of ZSTK474, a new phosphatidylinositol 3-kinase inhibitor. *J. Natl. Cancer Inst.*, **98**, 545–556 (2006).
19) Ohashi Y, Iijima H, Yamaotsu N, Yamazaki K, Sato S, Okamura M, Sugimoto K, Dan S, Hirono S, Yamori T. AMF-26, a novel inhibitor of the Golgi system, targeting ADP-ribosylation factor 1 (Arf1) with potential for cancer therapy. *J. Biol. Chem.*, **287**, 3885–3897 (2012).
20) Skehan P, Storeng R, Scudiero D, Monks A, McMahon J, Vistica D, Warren JT, Bokesch H, Kenney S, Boyd MR. New colorimetric cytotoxicity assay for anticancer-drug screening. *J. Natl. Cancer Inst.*, **82**, 1107–1112 (1990).
21) Monks A, Scudiero D, Skehan P, Shoemaker R, Paull K, Vistica D, Hose C, Langley J, Cronise P, Vaigro-Wolff A, Gray-Goodrich M, Campbell H, Mayo J, Boyd M. Feasibility of a high-flux anticancer drug screen using a diverse panel of cultured human tumor cell lines. *J. Natl. Cancer Inst.*, **83**, 757–766 (1991).
22) Paull KD, Shoemaker RH, Hodes L, Monks A, Scudiero DA, Rubinstein L, Plowman J, Boyd MR. Display and analysis of patterns of differential activity of drugs against human tumor cell lines: development of mean graph and COMPARE algorithm. *J. Natl. Cancer Inst.*, **81**, 1088–1092 (1989).
23) Eglen RM. Enzyme fragment complementation: a flexible high throughput screening assay technology. *Assay Drug Dev. Technol.*, **1**, 97–104 (2002).
24) Wallace S, Yang DJ, Deplessand E, Cherif A, Quadri S. High affinity tamoxifen derivatives. US6096874 (2000).
25) Weatherman RV, Clegg NJ, Scanlan TS. Differential SERM activation of the estrogen receptors (ERalpha and ERbeta) at AP-1 sites. *Chem. Biol.*, **8**, 427–436 (2001).
26) Rutanen EM, Heikkinen J, Halonen K, Komi J, Lammintausta R, Ylikorkala O. Effects of ospemifene, a novel SERM, on hormones, genital tract, climacteric symptoms, and quality of life in postmenopausal women: a double-blind, randomized trial. *Menopause*, **10**, 433–439 (2003).
27) Wallace OB, Richardson TI, Dodge JA. Estrogen receptor modulators: relationships of ligand structure, receptor affinity and functional activity. *Curr. Top. Med. Chem.*, **3**, 1663–1682 (2003).
28) Suh N, Glasebrook AL, Palkowitz AD, Bryant HU, Burris LL, Starling JJ, Pearce HL, Williams C, Peer C, Wang Y, Sporn MB. Arzoxifene, a new selective estrogen receptor modulator for chemoprevention of experimental breast cancer. *Cancer Res.*, **61**, 8412–8415 (2001).
29) Lewiecki EM. Lasofoxifene for the prevention and treatment of postmenopausal osteoporosis. *Ther. Clin. Risk Manag.*, **5**, 817–827 (2009).
30) Mountfield RJ, Kiehr B, John BA. Metabolism, disposition, excretion, and pharmacokinetics of levormeloxifene, a selective estrogen receptor modulator, in the rat. *Drug Metab. Dispos.*, **28**, 503–513 (2000).

31) Alexandersen P, Riis BJ, Stakkestad JA, Delmas PD, Christiansen C. Efficacy of levormeloxifene in the prevention of postmenopausal bone loss and on the lipid profile compared to low dose hormone replacement therapy. *J. Clin. Endocrinol. Metab.*, **86**, 755–760 (2001).

32) Rivera-Guevara C, Camacho J. Tamoxifen and its new derivatives in cancer research. *Recent Patents Anticancer. Drug Discov.*, **6**, 237–245 (2011).

Biochemical Pharmacology 86 (2013) 1272–1284

Contents lists available at ScienceDirect

Biochemical Pharmacology

journal homepage: www.elsevier.com/locate/biochempharm

Ridaifen-SB8, a novel tamoxifen derivative, induces apoptosis *via* reactive oxygen species-dependent signaling pathway

Wen-zhi Guo [a], Isamu Shiina [b], Yanwen Wang [b], Eri Umeda [b], Chihiro Watanabe [b], Shoko Uetake [b], Yoshimi Ohashi [a], Takao Yamori [a,c], Shingo Dan [a,*]

[a] Division of Molecular Pharmacology, Cancer Chemotherapy Center, Japanese Foundation for Cancer Research, 3-8-31 Ariake, Koto-ku, Tokyo 135-8550, Japan
[b] Department of Applied Chemistry, Faculty of Science, Tokyo University of Science, 1-3 Kagurazaka, Shinjuku-ku, Tokyo 162-860, Japan
[c] Center for Product Evaluation, Pharmaceuticals and Medical Devices Agency, 3-3-2 Kasumigaseki, Chiyoda-ku, Tokyo 100-0013, Japan

ARTICLE INFO

Article history:
Received 18 June 2013
Accepted 13 August 2013
Available online 22 August 2013

Keywords:
Tamoxifen-derivative
Ridaifen
Anticancer
Apoptosis
Drug discovery

ABSTRACT

Tamoxifen is an anticancer agent widely used for treatment of estrogen receptor (ERα)-positive breast cancer. We previously developed a novel synthesis of tamoxifen and its derivatives, named Ridaifens (RIDs). Some of them, including RID-SB8, exhibited a stronger anticancer activity than tamoxifen in ERα-positive MCF-7 cells while having lost the affinity for ERα, suggesting an ERα-independent anticancer mode of action. In this study, we investigated the underlying mechanism by which RID-SB8 exerts anticancer activity. As expected, anticancer activity of RID-SB8 was not influenced upon knockdown of ERα expression in MCF-7 cells. RID-SB8 exerted similar anticancer effects on thirteen ERα-negative cancer cell lines including human gliosarcoma SF539 cells. In SF539 cells, RID-SB8 triggered loss of mitochondrial membrane potential ($\Delta\Psi_m$) and progression of apoptosis accompanied by activation of caspases and translocation of apoptosis-inducing factor (AIF) to the nucleus. Furthermore, it induced reactive oxygen species (ROS), and a ROS scavenger, N-acetylcysteine (NAC), canceled loss of $\Delta\Psi_m$ and progression of apoptosis triggered by RID-SB8. Using fifteen human cancer cell lines, we demonstrated a significant correlation between RID-SB8 concentration required for ROS production and that required for cytotoxic effect across these cell lines, but such correlation was not observed for tamoxifen. Finally, the selective induction of ROS and cytotoxic effect on cancer cells by RID-SB8 were confirmed. From these results, we concluded that RID-SB8 exerts an anticancer effect *via* a mode of action distinct from tamoxifen, and that RID-SB8 could become a promising anticancer lead compound which selectively induces ROS formation and apoptosis in cancer cells.

1. Introduction

Tamoxifen is a selective estrogen receptor (ER) modulator (SERM), competing with estrogens for binding to ER, which is widely used in the chemotherapy of breast cancer [1–4]. It displays anticancer activity *via* the modulation of ERα-dependent gene expression, which results in the inhibition of proliferation [5,6]. Tamoxifen has also been shown to exhibit ERα-independent effects including modulation of signaling proteins such as protein kinase C (PKC), calmodulin, and the protooncogene c-myc. These effects are thought to be involved in the anticancer activity of tamoxifen in addition to ERα-dependent effects [7,8].

We previously developed a novel method for the synthesis of tamoxifen by a three-component coupling reaction [9,10]. Taking advantage of this reaction, we synthesized a series of tamoxifen derivatives designated as Ridaifens (RIDs) and tried to identify anticancer lead compounds that have potentially unique modes of action, not *via* modulation of ERα-dependent gene expression. To this end, we first examined RIDs for their ERα-binding activities and found that RIDs lacking either the phenyl group or the ethyl group at the C-2 position of the central ethylenic bond lost their affinity to ERα. Among these RIDs, we identified RID-SB8, which had completely lost ERα binding activity but had stronger cytotoxic activity in ERα-positive breast cancer MCF-7 cells [11]. However, the anticancer mechanism of RID-SB8 remained to be elucidated.

Anticancer agents often exert their anticancer effect by inducing apoptosis in cancer cells. During the apoptotic process, mitochondria are known to play an integral role. Mitochondrial

* Corresponding author. Tel.: +81 3 3570 0111x5432; fax: +81 3 3570 0484.
E-mail address: sdan@jfcr.or.jp (S. Dan).

0006-2952/$ – see front matter © 2013 Elsevier Inc. All rights reserved.
http://dx.doi.org/10.1016/j.bcp.2013.08.020

dysfunction occurs with an increase of outer mitochondrial membrane permeability [12,13] and loss of mitochondrial membrane potential ($\Delta\Psi_m$) [14–16]. In the classic apoptotic pathway, mitochondrial apoptotic components such as cytochrome *c* [17,18] are released from mitochondria followed by interaction with apoptotic proteinase-activating factor-1 and procaspase-9 (18) to form apoptosomes. The latter activation of procaspase-9 results in activation of downstream effector caspases such as caspase-3 and 7 [19,20]. This activation of caspase causes the proteolytic cleavage of substrates such as poly (ADP-ribose) polymerase-1 (PARP) [21,22] and inhibitor of caspase-dependent DNase (ICAD) [23] and eventual cell death. On the other hand, apoptosis can also occur through an alternative mitochondrial route, which is independent of caspase activation. For example, apoptosis is mediated by the disruption of the $\Delta\Psi_m$ and the translocation of apoptosis-inducing factor (AIF) from the mitochondria to the nucleus, where it plays an essential role in chromatin condensation and/or large-scale DNA degradation [24–26].

Reactive oxygen species (ROS) are the byproducts of normal cellular oxidative processes and are believed to play an important role during apoptosis induction [27–29]. Many anticancer drugs that induce the production of intracellular ROS have been reported [27]. ROS can directly result in activation of the mitochondrial membrane permeability and loss of $\Delta\Psi_m$ [30]. Recent reports have shown that cancer cells possess higher levels of ROS than normal cells and the increased dependence of cancer cells on the ROS stress-response pathway may be the basis for the selectivity of cell death [31,32]. Therefore, selective killing of cancer cells by targeting the stress response to ROS has become a novel approach to treat cancer.

In the present study, we regarded RID-SB8 as a promising anticancer lead compound and demonstrated its synthesis. Furthermore, we studied the underlying mechanisms by which RID-SB8 exerts its ERα-independent anticancer effect. In particular, its cytotoxic effects on mitochondrial apoptosis progression *via* ROS production on cancer cells and primary normal cells were examined.

2. Materials and methods

2.1. Reagents

All reagents were purchased from Sigma (St. Louis, MO), unless otherwise specified.

2.2. Preparation of RID-SB8

2.2.1. 4,4′-Bis[2-(pyrrolidin-1-yl)ethoxy]phenyl ketone (RID-SB5) (3)

To a solution of 4,4′-dihydroxybenzophenone (**2**) (262 mg, 1.22 mmol) in DMF (12.2 mL) was added 55% sodium hydride (dispersion in paraffin liquid, 428 mg, 9.81 mmol). The reaction mixture was stirred for 15 min at 50 °C and then 1-(2-chloroethyl)pyrrolidine hydrochloride (688 mg, 4.05 mmol) was added in portions at room temperature. After the reaction mixture had been stirred for 7.5 h at 50 °C, saturated aqueous ammonium chloride was added at 0 °C. The mixture was extracted with dichloromethane, and the organic layer was washed with water and brine, and dried over sodium sulfate. After filtration of the mixture and evaporation of the solvent, the crude product was purified by column chromatography on silica (eluant; ammoniacal chloroform/methanol = 9/1) to afford **3** (425 mg, 85%) as a pale yellow solid: Mp: 109.8–110.5 °C; IR (KBr): 2962, 2796, 1643, 1601, 1512, 1477, 1319, 1261, 1250 cm^{-1}; ^1H NMR ($CDCl_3$): δ 7.81–7.72 (m, 4H, Ar), 7.03–6.91 (m, 4H, Ar), 4.20 (t, J = 6.0 Hz, 4H, OCH_2), 2.95 (t, J = 6.0 Hz, 4H, NCH_2), 2.72–2.56 (m, 8H, pyrrolidinyl 2-H), 1.89–1.76 (m, 8H, pyrrolidinyl 3-H); ^{13}C NMR ($CDCl_3$): δ 194.2 (1), 161.8, 132.0, 130.7, 113.9 (Ar), 66.8 (OCH_2), 54.64 (NCH_2), 54.55 (pyrrolidinyl 2-C), 23.3 (pyrrolidinyl 3-C); HR MS: calcd for $C_{25}H_{33}N_2O_3$ ($M+H^+$) 409.2486, found 409.2486.

2.2.2. 1,1-Bis{4-[2-(pyrrolidin-1-yl)ethoxy]phenyl}heptanol (RID-SB6) (4)

To a solution of **3** (484 mg, 1.19 mmol) in THF (11.8 mL) at −10 °C was added *n*-butyllithium in *n*-hexane (2.54 M, 1.17 mL, 2.97 mmol). After the reaction mixture had been stirred for 17.5 h at room temperature, saturated aqueous ammonium chloride was added at 0 °C. The mixture was extracted with dichloromethane, and the organic layer was washed with brine and dried over sodium sulfate. After filtration of the mixture and evaporation of the solvent, the crude product was purified by thin layer chromatography on silica (eluant; ammoniacal chloroform/methanol = 9/1) to afford **4** (507 mg, 92%) as a pale yellow solid: Mp: 37.5–38.0 °C; IR (KBr): 3402, 2954, 2935, 2873, 2808, 1608, 1508, 1246 cm^{-1}; ^1H NMR ($CDCl_3$): δ 7.32–7.22 (m, 4H, Ar), 6.88–6.78 (m, 4H, Ar), 4.08 (t, J = 6.0 Hz, 4H, OCH_2), 2.87 (t, J = 6.0 Hz, 4H, NCH_2), 2.65–2.54 (m, 8H, pyrrolidinyl 2-H), 2.23–2.16 (m, 2H, 2-H), 1.86–1.72 (m, 8H, pyrrolidinyl 3-H), 1.32 (tt, J = 7.5, 7.5 Hz, 2H, 3-H), 1.29–1.16 (m, 2H, 4-H), 0.86 (t, J = 7.5 Hz, 3H, 5-H); ^{13}C NMR ($CDCl_3$): δ 157.4, 139.8, 127.2, 113.9 (Ar), 77.6 (1), 66.7 (OCH_2), 55.0 (NCH_2), 54.6 (pyrrolidinyl 2-C), 42.0 (2), 26.0 (3), 23.4 (pyrrolidinyl 3-C), 23.1 (4), 14.1 (5); HR MS: calcd for $C_{29}H_{43}N_2O_3$ ($M+H^+$) 467.3268, found 467.3270.

2.2.3. 1,1-Bis{4-[2-(pyrrolidin-1-yl)ethoxy]phenyl}hept-1-ene (RID-SB8) (1)

To a solution of **4** (197 mg, 0.422 mmol) in benzene (15.0 mL) at room temperature was added *p*-toluenesulfonic acid monohydrate (121 mg, 0.636 mmol). After the reaction mixture had been stirred for 7.5 h at 110 °C, saturated aqueous sodium hydrogen carbonate was added at 0 °C. The mixture was extracted with diethyl ether, and the organic layer was dried over sodium sulfate. After filtration of the mixture and evaporation of the solvent, the crude product was purified by thin layer chromatography on silica (eluant; ammoniacal chloroform/methanol = 15/1) to afford **1** (146 mg, 77%) as a pale yellow oil: IR (neat): 2958, 2927, 1959, 1604, 1508, 1450, 1385, 1242 cm^{-1}; ^1H NMR ($CDCl_3$): δ 7.19–7.01 (m, 4H, Ar), 6.95–6.85 (m, 2H, Ar), 6.85–6.75 (m, 2H, Ar), 5.93 (t, J = 7.2 Hz, 1H, 2-H), 4.13 (t, J = 6.0 Hz, 2H, OCH_2), 4.08 (t, J = 6.0 Hz, 2H, OCH_2), 2.92 (t, J = 6.0 Hz, 2H, NCH_2), 2.88 (t, J = 6.0 Hz, 2H, NCH_2), 2.71–2.53 (m, 8H, pyrrolidinyl 2-H), 2.08 (dt, J = 7.2, 7.2 Hz, 2H, 3-H), 1.89–1.72 (m, 8H, pyrrolidinyl 3-H), 1.44 (tq, J = 7.2, 7.5 Hz, 2H, 4-H), 0.89 (t, J = 7.5 Hz, 3H, 5-H); ^{13}C NMR ($CDCl_3$): δ 157.8, 157.6, 140.5, 136.0, 132.9, 131.0, 128.24, 128.24, 128.16, 114.0 (Ar, 1, 2), 66.9, 66.8 (OCH_2), 55.1, 55.0 (NCH_2), 54.69, 54.66 (pyrrolidinyl 2-C), 31.8 (3), 23.45, 23.42 (pyrrolidinyl 3-C), 23.3 (4), 13.9 (5); HR MS: calcd for $C_{29}H_{41}N_2O_2$ ($M+H^+$) 449.3163, found 449.3165 (Fig. 1).

2.3. Cell lines and cell culture

The following cancer cells from the JFCR39 panel [33–35] of human cancer cell lines and normal epithelial cells obtained from Lonza (Walkersville, MD) were used in this study. Breast cancer, MCF-7, MDA-MB-231; ovarian cancer, SK-OV3; lung cancer, NCI-H23 and NCI-H226; colorectal cancer, HCC-2998 and HT-29; glioma, SF295, SF539, SNB75 and SNB78; prostate cancer, DU-145 and PC-3; Renal cancer, RXF-631L and ACHN. All the cancer cell lines were cultured in RPMI 1640 medium supplemented with 5% (v/v) fetal bovine serum, penicillin (100 U/mL) and streptomycin (100 μg/mL) at 37 °C in a humidified atmosphere containing 5% (v/v) CO_2. Normal Human Mammary Epithelial Cells (HMEC) and

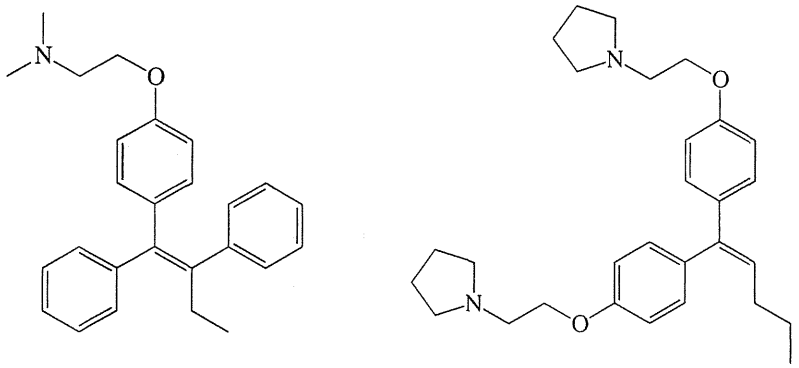

Fig. 1. Chemical structures of tamoxifen and RID-SB8.

Normal Human Renal Proximal Tubule Epithelial Cells (RPTEC) were cultured in mammary epithelial growth medium (MEGM Bullet Kit; Lonza Corporation) and renal epithelial growth medium (REGM Bullet Kit; Lonza Corporation) respectively at 37 °C in a humidified atmosphere containing 5% (v/v) CO_2.

2.4. WST-8 assay

Cell viability was determined using WST-8 assay kit (Kishida Chemicals, Osaka, Japan) as described previously [36]. Briefly, cells were cultured in 96-well plates and treated on the second day with the agents indicated for 24 h. After the addition of 10 μL of water-soluble tetrazolium salt (WST-8) for 2 h, the conversion of WST-8 into formazan was measured using a microplate spectrophotometer (Benchmark Plus™, Bio Rad, Hercules, CA) at 450-nm absorbance.

2.5. Caspase-3/7 activity assay

Caspase-3/7 activity was measured by the Caspase-Glo assay kit (Promega, Madison, USA). Briefly, cells grown in 96-well white plates were treated with agents for 12 h. Subsequently, 100 μL of Caspase-Glo reagent was added to each well. After gentle mixing by a plate shaker, the plate was then incubated at room temperature for 2 h. The luminescence was measured using a plate-reading luminometer (EnVision, Boston, MA). The experiments were performed in triplicate and repeated on two separately-initiated cultures.

2.6. Flow cytometric analysis

Evaluation of the cell cycle distribution and sub-G1 peaks by flow cytometric analysis was performed as described previously [37]. Briefly, cells grown in 12-well plates were collected by trypsinization, washed twice with PBS, and fixed with 80% ethanol on ice for 1 h. Subsequently, the cells were incubated in 10 μg/mL RNase A for 30 min at 37 °C followed by the staining in propidium iodide (PI) (Sigma) solution (50 μg/mL) for 15 min at room temperature in the dark. Then cells were analyzed by flow cytometer (FACS Calibur, BD biosciences, USA).

2.7. Annexin V/propidium iodide (PI) assay for apoptosis

Annexin V and PI staining was used for detection of apoptosis. The Annexin V/PI double-staining method was used according to the manufacturer's protocol (BD Pharmingen, Bedford, MA). Briefly, Cells grown in 12-well plates were collected by trypsinization, washed twice with PBS and stained with 5 μL of Annexin V-FITC and 5 μL of PI (5 μg/mL) in binding buffer for 15 min at room temperature in the dark. The apoptotic cells were determined by flow cytometer (FACS Calibur).

2.8. Western blotting

Western blotting was performed as described previously [38]. Briefly, cells were lysed with a lysis buffer containing 10 mM Tris–HCl (pH 7.4), 50 mM Na-orthovanadate (Na_3VO_4), 30 mM Na-pyrophosphate, 50 mM NaF, 50 mM NaCl, 5 mM EDTA, 0.5% NP-40, and protease inhibitors. The cell lysates were centrifuged at 15,000 × *g* for 30 min at 4 °C, and the supernatant was treated with SDS sample buffer following separation using electrophoresis on a 4–20% (w/v) gel. Proteins were transferred to a nitrocellulose membrane and the membrane was blocked with 1:5 diluted Odyssey blocking buffer (LI-COR Biosciences, Lincoln, NE). Subsequently, the membrane was incubated with anti-ERα (SC-8002), ERβ (SC-8974) antibodies (Santa Cruz Biotechnology, Inc., Santa Cruz, CA, USA), anti-Complex IV (COXIV) (A-6404) antibody (Invitrogen), anti-PARP (#9542), cleaved caspase-3 (#9664), cleaved caspase-9 (#7237), AIF (#4642), Histone H3 (#4499), actin (#4976) antibodies (Cell signaling Technology, MA, USA). After the incubation in Alexa Fluor 680 goat anti-rabbit IgG or anti-mouse IgG secondary antibodies, specific signals were detected using the Odyssey Infrared Imaging System (LI-COR Biosciences).

2.9. Preparation of mitochondrial and nuclear fractions

For determination of the translocation of AIF from mitochondria to nucleus, mitochondrial and nuclear fractions were prepared with Mitochondria Isolation kit (MitoSciences, Eugene, OR) according to the manufacturer's protocol. Cells were collected by trypsinization, washed twice, suspended in 250 μL Reagent A and then incubated on ice for 10 min. After 30 strokes of homogenization with Pestle B, cells were centrifuged at 1000 × *g* for 10 min at 4 °C. The cell pellet was saved as the nuclear fraction. The supernatant was further centrifuged at 12,000 × *g* for 15 min at 4 °C and the resulting pellet suspended in Reagent C containing protease inhibitors was used as the mitochondrial protein fraction. Complex (COX) IV (mitochondrial marker) and Histone-H3 (nuclear marker) were used to determine the purity of the fractions.

2.10. Mitochondrial membrane potential ($\Delta\Psi_m$) assay

$\Delta\Psi_m$ was determined using a fluorescent probe-5,5′,6,6′-tetrachloro-1,1′,3,3′-tetraethylbenzimidazolyl-carbocyanine iodide

(JC-1) (Molecular Probes, Eugene, OR). After agent treatment, cells in 12-well plates were exposed to JC-1 (2 μM) for 20 min at 37 °C. The cells were collected by trypsinization, washed twice, suspended in 300 μL PBS. JC-1 signal was detected using a flow cytometer (FACS Calibur) at 530 nM (FL-1, green) and 590 nM (FL-2, red). The ratio of red *versus* green fluorescence was measured and expressed as $\Delta\Psi_m$.

2.11. Immunofluorescence microscopy

The translocation of AIF was observed by fluorescence microscopy as described previously [39]. After being cultured in a 24-well glass bottom plate for 16 h and treated with the drug for the indicated period, cells were exposed to 0.2 μM MitoTracker Red (Molecular Probes) for 30 min. Subsequently, cells were washed with PBS twice, fixed with cold 3.8% paraformaldehyde in PBS (Wako Pure Chemical Industries, Osaka, Japan) for 20 min, and then washed and permeabilized with 0.4% Triton X-100 (Sigma) in PBS for 10 min at room temperature. Cells were incubated in blocking buffer containing 1% BSA and 2% normal goat serum (Dako, Glostrup, Denmark) for 30 min before overnight incubation at 4 °C with anti-AIF antibody diluted in blocking buffer. After being washed, cells were incubated for 1 h with secondary antibodies. Cells were then washed, stained with DAPI (Molecular Probes), and mounted with fluorescent mounting medium (Dako). The immunostained cells were imaged using a fluorescent microscope IX81 (Olympus Corp., Tokyo, Japan) and Meta Morph Software (Molecular Devices, Sunnyvale, CA).

2.12. Knockdown of ERα and AIF

ERα siRNA and AIF siRNA duplexes with Stealth™ modification against human *ERα*, and *AIF* were purchased from Invitrogen. The sense (top) sequences of ERα siRNA 1 and ERα siRNA 2 were 5′-CAUACUUCCCUUGUCAUUGGUACUG-3′ and 5′-CCACCUUCUAGA-AUGUGCCUGGCUA-3′, respectively. The siRNA sense (top) sequences of AIF siRNA 1 and AIF siRNA 2 were 5′-CCAAGUCAU-GUUCCUUUCCUGCUAA-3′ and 5′-GGAGAUGC-UGCAUGCUUC-UACGAUA-3′, respectively. As a negative control (NC), the random sequence, 5′-CAGUUACUCCGUCUAGUCU-3′, was used. Cells were transfected with the above described siRNA using Lipofectamine 2000 (Invitrogen). Two days after transfection, the cells were harvested and used for each assay.

2.13. ROS detection

ROS was detected by staining the cells with CM-H_2DCFDA (Molecular Probes). After incubation with agent for the indicated times, cells were incubated with 10 μM CM-H_2DCFDA for 30 min. The fluorescent intensity was recorded by excitation at 485 nm and emission at 535 nm using an EnVision microplate reader (PerkinElmer, MA, USA).

2.14. Statistical analysis

Quantitative data were represented as means ± SD from three independent experiments, and p values were analyzed using the Student's t-test. Pearson correlation coefficients were calculated for

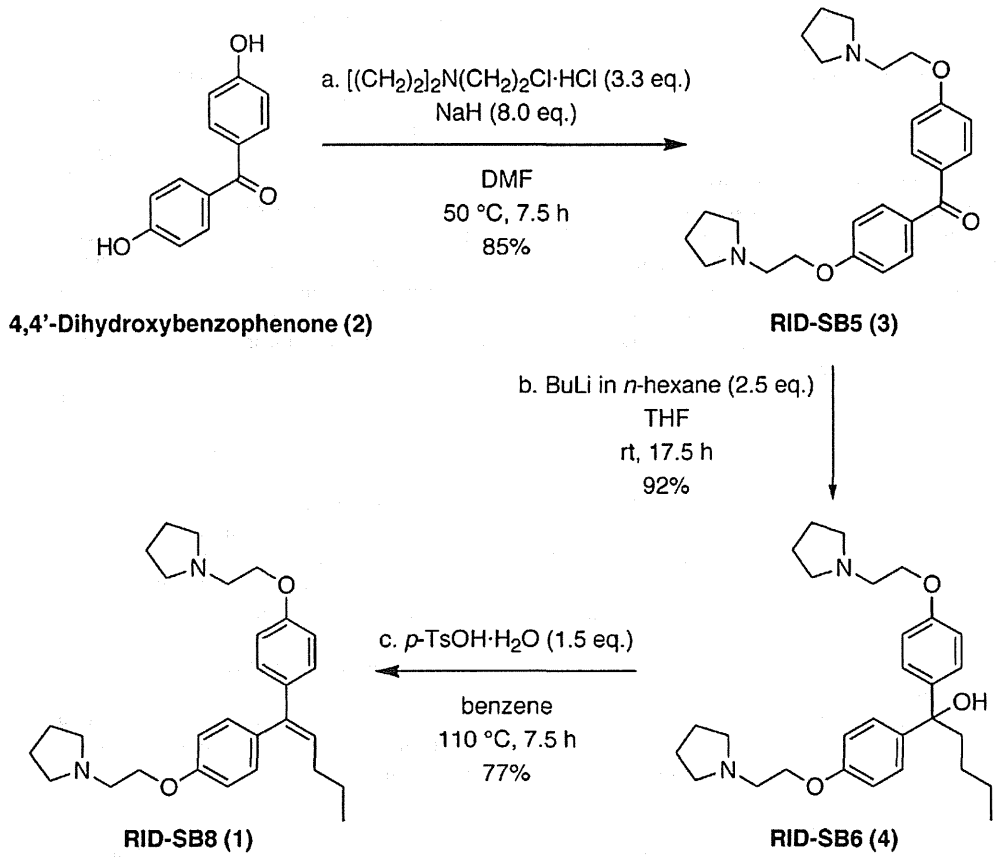

Fig. 2. Synthesis of RID-SB8 (**1**) from 4,4′-Dihydroxybenzophenone (**2**).[a]
[a]Reagents and conditions: (a) [$(CH_2)_2$]$_2$N(CH_2)$_2$Cl·HCl (3.3 eq.), NaH (8.0 eq.), DMF, 50 °C, 7.5 h, 85%; (b) BuLi in n-hexane (2.54 M, 2.5 eq.), THF, room temperature, 17.5 h, 92%; (c) p-TsOH·H_2O (1.5 eq.), benzene, 110 °C, 7.5 h, 77%.

statistical correlation between the cytotoxic activities and ROS inducing activities of RID-SB8 across fifteen cancer cell lines.

3. Results

3.1. Synthesis of RID-SB8 (1) from 4,4′-Dihydroxybenzophenone (2)

RID-SB8 (**1**), 1,1-bis{4-[2-(pyrrolidin-1-yl)ethoxy]phenyl}-hept-1-ene, was synthesized from 4,4′-dihydroxybenzophenone (**2**) *via* a chemical approach consisting of *O*-alkylation, C4 segment installation, and the acid-mediated dehydration as shown in Fig. 2. First, the phenol moieties in **2** were transformed into the corresponding aminoethyl ethers in 85% yield by alkylation with 1-(2-chloroethyl)pyrrolidine hydrochloride in dimethylformamide (DMF), and the successive alkylation of the carbonyl group in **3** using butyllithium was carried out in tetrahydrofuran (THF) to provide 1,1-diphenylpentanol derivative **4** in 92% yield. Finally, treatment of the tertiary alcohol **4** with *p*-TsOH was attempted in benzene and the facile dehydration process successfully furnished to afford the desired molecule **1** in 77% yield. Thus, an efficient method for the preparation of **1** was established through three steps with 60% overall yield from the commercially available **2**.

3.2. Anticancer activity of RID-SB8 and tamoxifen on MCF-7 cells

First, we examined the effect of RID-SB8 on the viability of MCF-7 cells. After 24 h incubation, RID-SB8 had markedly decreased the viability of MCF-7 at concentrations as low as 4 μM (Fig. 3A), whereas tamoxifen needed a treatment concentration of approximately 18 μM to achieve a similar effect (Fig. 3A). The estimated IC_{50} (50% inhibition concentrate) doses of RID-SB8 and tamoxifen were approximately 3.04 μM and 12.1 μM, respectively. In our previous study, we demonstrated that with the modification of the tamoxifen structure, RID-SB8 completely lost ERα binding activity [11], suggesting that RID-SB8 does not target ERα. To further clarify whether the cytotoxic activity of RID-SB8 is independent of the ERα expression, knockdown of ERα in MCF-7 was carried out by transfection of ERα siRNA. The ERα siRNA treatment resulted in the obvious reduction of ERα protein amount to about 10% of the control siRNA treatment (Fig. 3B). Using these cells, the sensitivity to RID-SB8 and tamoxifen were examined. As shown in Fig. 3C, in ERα siRNA-treated MCF-7, anticancer activity of tamoxifen was partially blocked by expression knockdown of ERα, whereas the activity of RID-SB8 showed no alteration. These results indicated that RID-SB8 exerted higher anticancer activity on MCF-7 cells than tamoxifen, and the activity was ERα-independent.

3.3. RID-SB8 induces apoptosis in SF539 cells

As shown previously, RID-SB8 displays a broad-spectrum cytotoxic activity across 39 human cancer cell lines, known as JFCR39. Among the JFCR39 cell lines, a glioma cell line, SF539, exhibited the highest sensitivity to RID-SB8 [11], therefore, we used SF539 cells in our subsequent research. RID-SB8 effectively reduced the cell viability of SF539 in a dose-dependent manner (IC_{50} = 2.10 μM) (Fig. 4A). Then, we determined whether RID-SB8 induces cell death *via* apoptosis in SF539 using flow cytometric analysis. As shown in Fig. 4B, treatment with RID-SB8 for 18 h caused a significant increase in the sub-G1 population in a dose-dependent manner. Furthermore, we found that treatment with

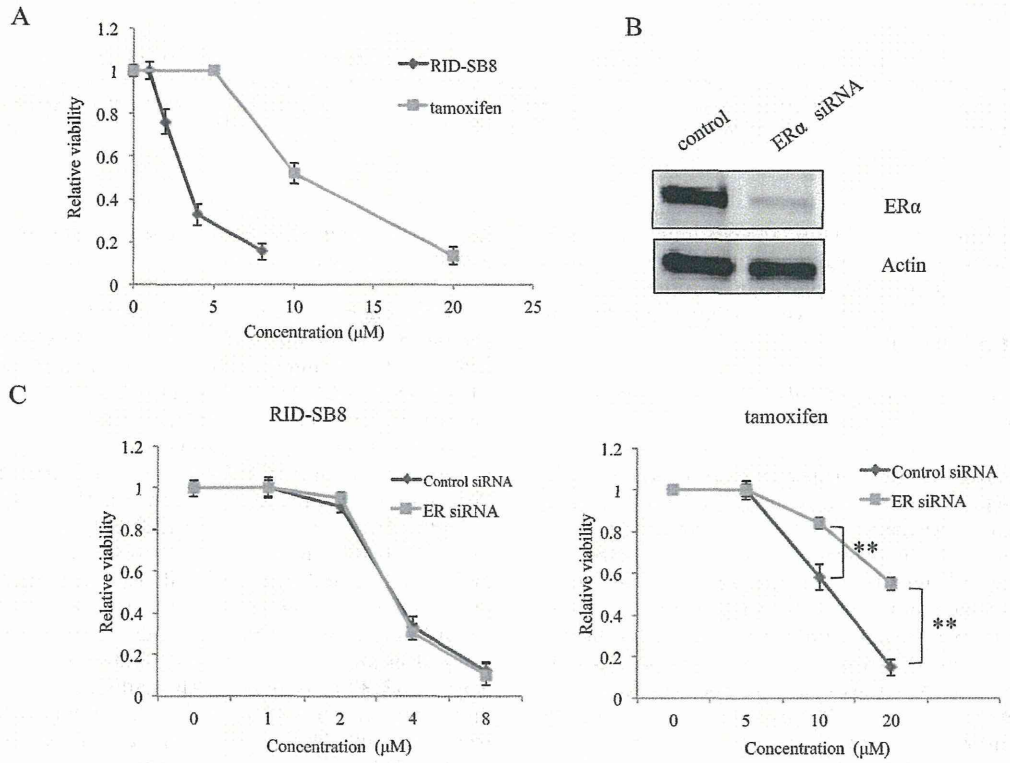

Fig. 3. Cytotoxic activity of RID-SB8 in ER-independent manner in MCF-7. (A) Cell viability of MCF-7 was analyzed using WST-8 assay. Cells were treated with 1, 2, 4, 8 μM RID-SB8 or 5, 10, or 20 μM tamoxifen for 24 h. 0.05% DMSO was used as the vehicle control. Results represent the means ± SD from three independent experiments. (B) Cell lysates were prepared 48 h after ERα siRNA transfection, and analyzed by Western blotting, as described in Section 2. (C) After transfection of ERα siRNA for 48 h, cells were replanted in dish. Drug treatment and WST assay were the same as described in (A). Results represent the means ± SD from three independent experiments. Differences with $p < 0.01$ (**) are considered statistically significant.

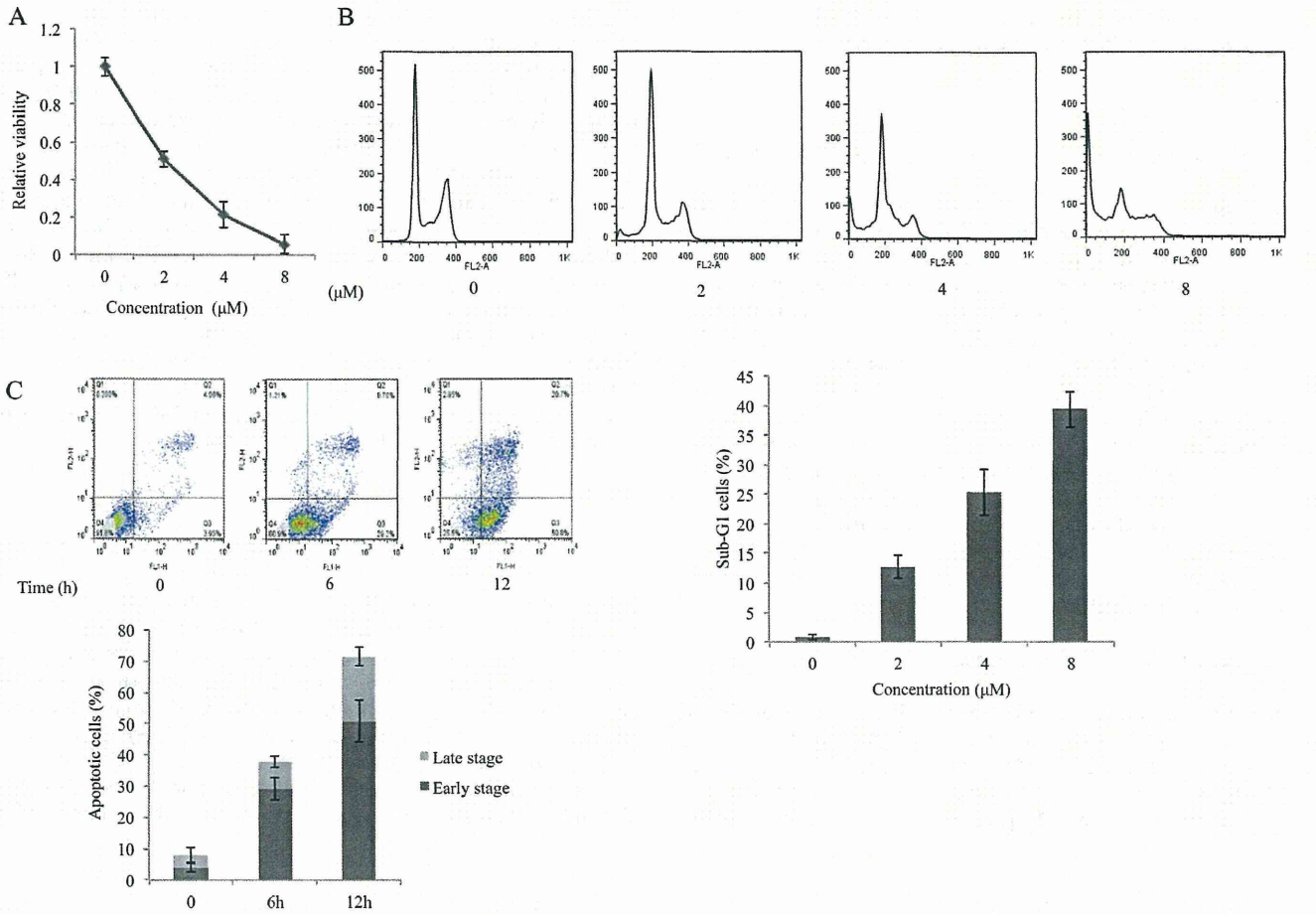

Fig. 4. Apoptotic cell death induced by RID-SB8. (A) Cell viability of SF539. Cells were treated with 2, 4, 8 μM RID-SB8 for 24 h followed by WST-8 assay. (B) RID-SB8 induced apoptosis in a dose-dependent manner. SF539 cells were treated with 2, 4, 8 μM RID-SB8 for 18 h. Apoptosis was analyzed as a sub-G1 fraction by FACS. (C) SF539 cells were treated with 8 μM RID-SB8 for 6 and 12 h, harvested, and stained with Annexin V and PI. Cell death was determined by flow cytometry. *Bottom right quadrant*, Annexin V (+) and PI (−), cells in early stage of apoptosis; *top right quadrant*, Annexin V (+) and PI (+), cells in late stage of apoptosis. All the results represent the means ± SD from three independent experiments.

4 μM RID-SB8 increased the population of cells in both the early stage (Annexin V positive and PI negative) and late stage (Annexin V positive and PI positive) of apoptosis in a time-dependent manner (Fig. 4C). From these results, we concluded that RID-SB8 induced cell death *via* apoptosis.

3.4. RID-SB8-induced apoptosis is partially mediated by caspase-dependent pathway

We next examined whether caspase activation was involved in RID-SB8-induced apoptosis. Treatment with RID-SB8 resulted in a marked increase in caspase-3/7 activity in a dose-dependent manner compared with the control (Fig. 5A). As expected, the expression of active cleaved forms of caspase-3, caspase 9 and PARP were detected by immunoblot analysis (Fig. 5B). Moreover, pretreatment with a pan-caspase inhibitor, Z-VAD-FMK, for 1 h prevented loss of cell viability after exposure to RID-SB8 (Fig. 5C), although the effect was only partial. Similar results were obtained in the Annexin V/PI assay and Flow cytometric analysis, the apoptotic cells (Annexin V positive) and sub-G1 cells induced by 8 μM RID-SB8 was only partially reduced (Fig. 5D and E). These results suggest that RID-SB8-induced apoptosis was partially mediated by a caspase-dependent pathway, and that caspase-independent apoptosis was also involved in this process.

3.5. RID-SB8-induced caspase-independent apoptosis is through the translocation of AIF

Mitochondrial dysfunction characterized by loss of $\Delta\Psi_m$ is known to play an important role in apoptosis. We measured the $\Delta\Psi_m$ by JC-1 staining in SF539 cells treated with RID-SB8. As shown in Fig. 6A, treatment with RID-SB8 for 12 h obviously decreased the $\Delta\Psi_m$. This result revealed that RID-SB8 actually caused the mitochondrial dysfunction.

The involvement of AIF in a caspase-independent mitochondrial apoptotic pathway is well known. We therefore determined whether AIF played a role in RID-SB8-induced apoptosis. We found that RID-SB8 caused the reduction of AIF expression in mitochondria and increase in AIF expression in the nucleus in a dose-dependent manner, suggesting the release of AIF from mitochondria to nucleus (Fig. 6B). Then, we examined the translocation of AIF by immunofluorescence microscopy. The control SF539 cells showed AIF staining in a punctured pattern, indicating the normal location in mitochondria. In contrast, cells exposed to RID-SB8 for 16 h resulted in increased diffuse staining of AIF in the nucleus (Fig. 6C). This result clearly showed the translocation of AIF from mitochondria to nucleus by the treatment of RID-SB8. In addition, pretreatment with Z-VAD-FMK did not affect the translocation of AIF (Fig. 6C), indicating the AIF translocation is caspase-independent. In the same assay,

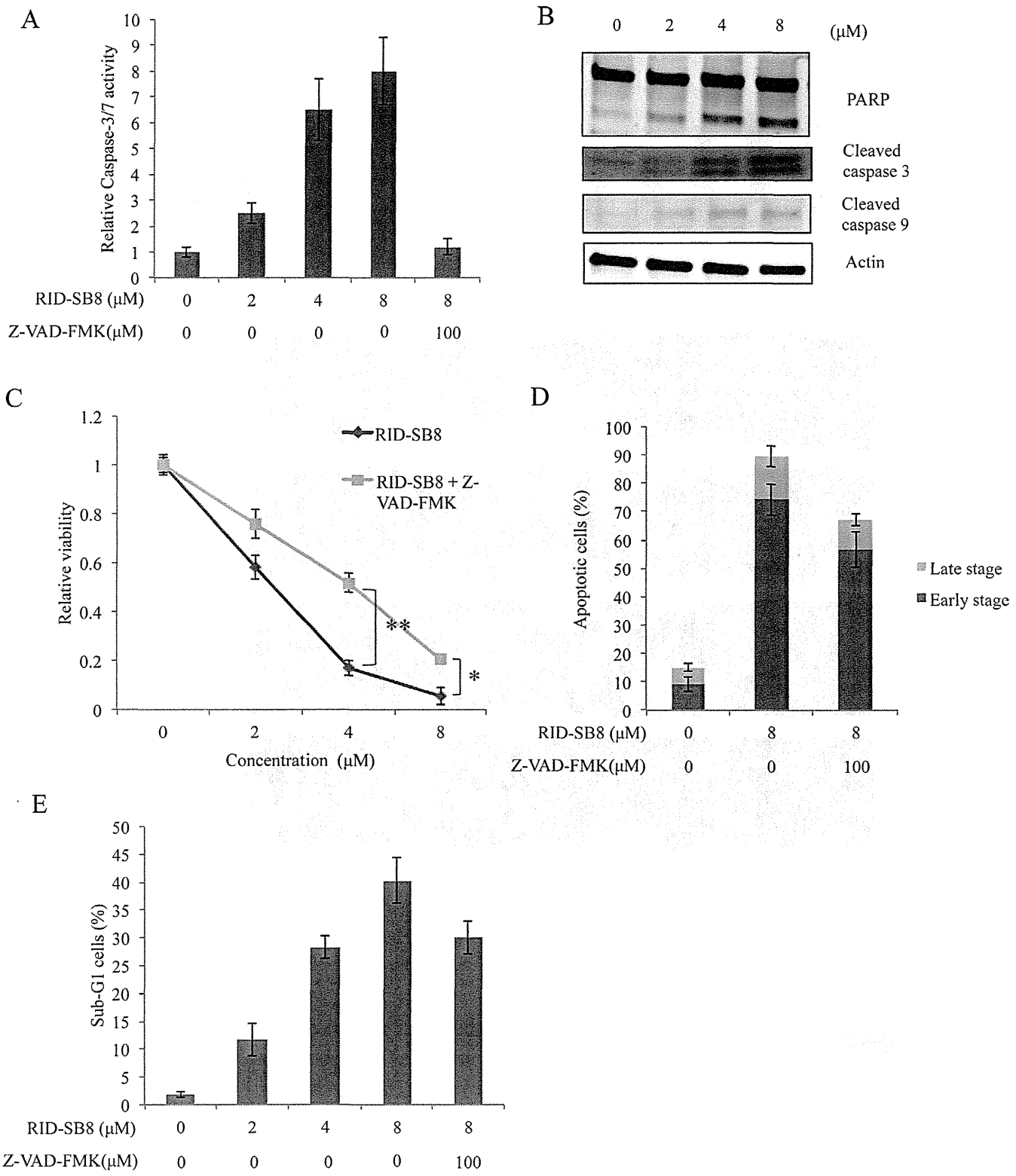

Fig. 5. RID-SB8-induced apoptosis is partially mediated by caspase-dependent pathway. (A) SF539 cells grown in a white wall 96-well plate were treated with 2, 4, 8 μM RID-SB8 for 12 h, followed by adding 100 μL of Caspase-Glo reagent. After incubation at room temperature for 2 h, the fluorescence intensity was recorded by microplate reader. Results represent the means ± SD from three independent experiments. (B) Cell lysates were prepared after 24 h incubation with RID-SB8 and analyzed by Western blotting, as described in Section 2. (C) Cells were pretreated with or without 100 μM Z-VAD-FMK for 1 h before exposed to RID-SB8, followed by WST-8 assay for cell viability, (D) annexin V/PI assay and E, flow cytometric analysis annexin V/PI assay for apoptosis, as described in Section 2. Results of C, D, E represent the means ± SD from three independent experiments. Differences with $p < 0.05$ (*) or $p < 0.01$ (**) are considered statistically significant.

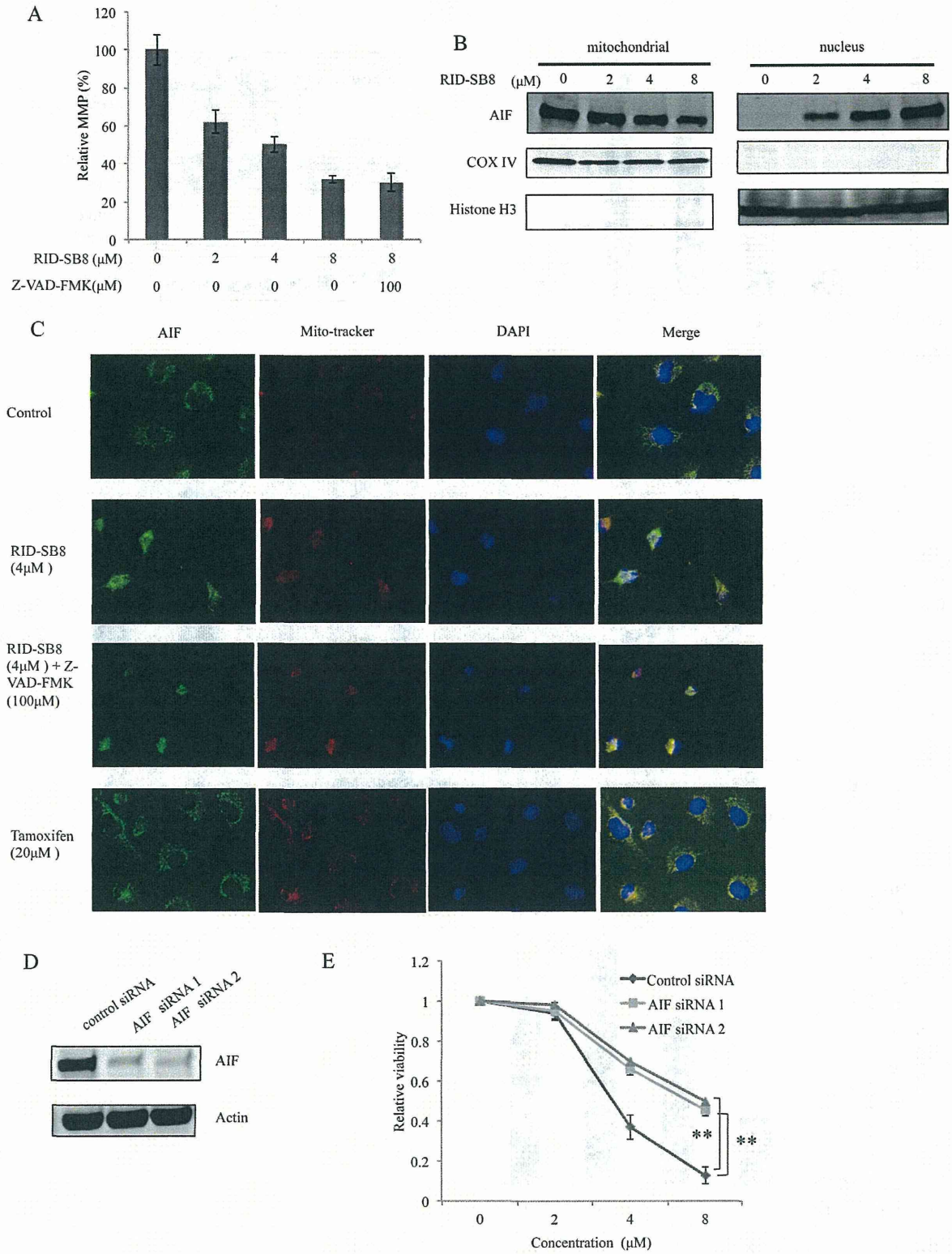

Fig. 6. AIF translocation is involved in RID-SB8-induced apoptosis. (A) The effect of RID-SB8 on MMP. SF539 cells were treated with the indicated concentrations of RID-SB8 before the MMP was measured by uptake of JC-1 using flow cytometry. *Columns*, mean of three individual experiments; *bars*, SD. (B) After treatment of RID-SB8 for 16 h, mitochondrial and nuclear fractions were prepared as described in Section 2 and subjected to immunoblot analysis. COX IV and Histone H3 were used as marker proteins of mitochondria and nucleus respectively to identify the purity of the mitochondrial fraction and the nuclear fraction. (C) SF539 cells growing in a glass bottom plate were pretreated with or without 100 μM Z-VAD-FMK for 1 h before being exposed to 4 μM RID or 20 μM tamoxifen for 16 h. Then, AIF, mitochondria and nucleus were labeled with anti-AIF antibody, MitoTracker and DAPI, respectively, followed by observation using a fluorescence microscope. (D) Cell lysates were prepared 48 h after AIF siRNA transfection, and analyzed by Western blotting. (E) After transfection of AIF siRNA for 48 h, cells were replanted in the dish. After treatment with RID-SB8 for 24 h, cell viability was determined by WST-8 assay. Results represent the means ± SD from three independent experiments. Differences with $p < 0.01$ (**) are considered statistically significant.

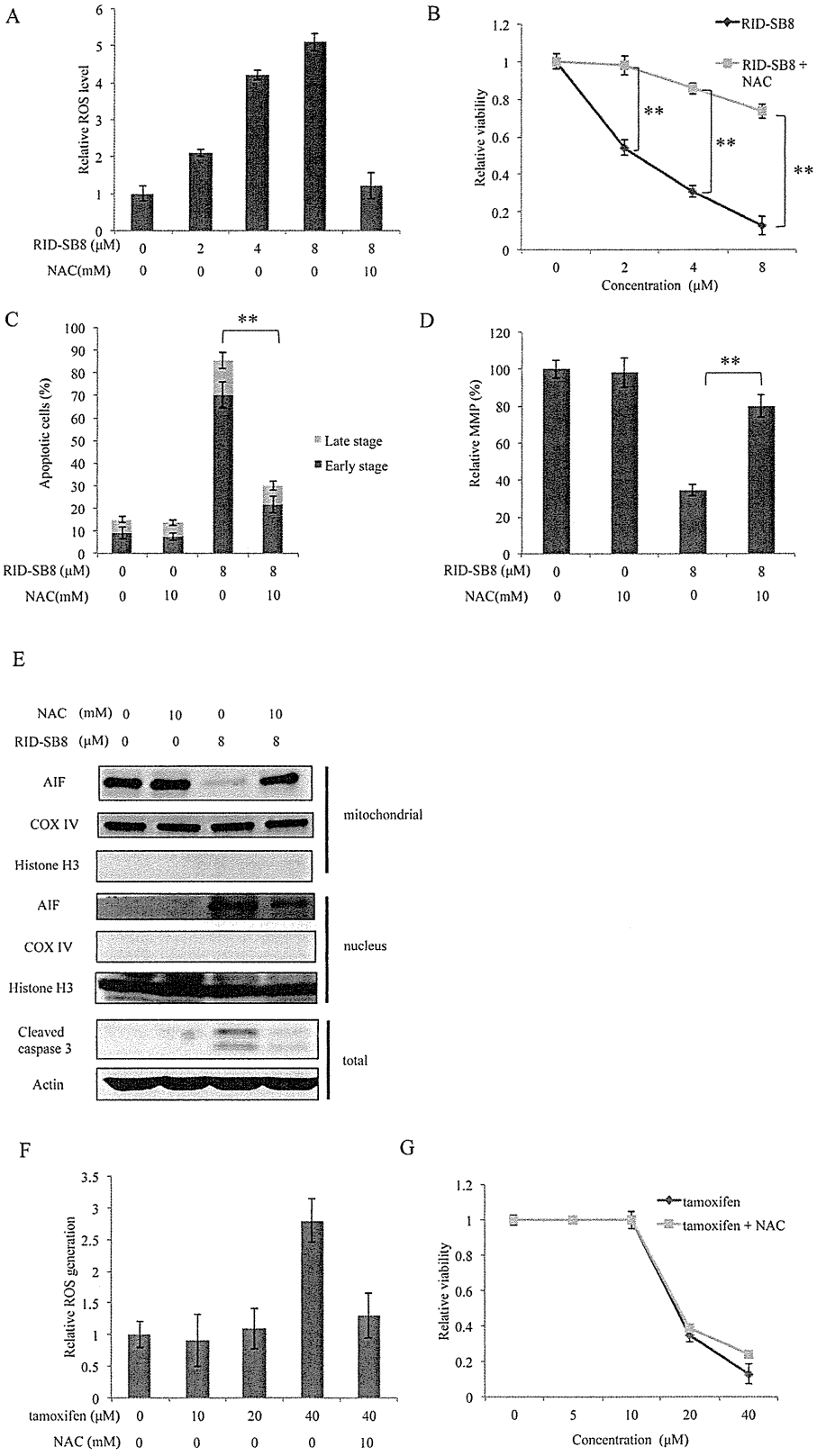

Fig. 7. ROS play an essential role in RID-SB8-induced apoptosis. SF539 cells were pretreated with or without 10 mM NAC for 1 h. Then, (A) SF539 cells growing in black 96-well plate were exposed to RID-SB8 for 2 h. Subsequently, cells were loaded with CM-H_2DCFDA for 30 min, followed by dectection using a microplate reader. (B) Cell viability after treatment with RID-SB8 for 24 h was determined by WST-8 asssay. (C) SF539 cells were treated with 8 μM RID-SB8 for 12 h, harvested, and stained with Annexin V and PI. Apoptotic cells was determined by flow cytometry. (D) SF539 cells were treated with 8 μM RID-SB8 before the MMP was measured by uptake of JC-1 using flow cytometry. (E) After treatment with RID-SB8 for 16 h, mitochondrial and nuclear fractions were prepared as described in Section 2 and subjected to immunoblot analysis. (F) SF539 cells were exposed to indicated concentrations of tamoxifen for 2 h, ROS generation was determined as described in (A). (G) Cell viability after treatment with RID-SB8 for 24 h was determined by WST-8 asssay. All the results except for (E) represent the means ± SD from three independent experiments. Differences with $p < 0.01$ (**) are considered statistically significant.